ISSN : 0973 - 0613

JOURNAL OF WIND & ENGINEERING

Vol. 8 No. 2 July 2011

CONTENTS

Published by: Indian Society for Wind Engineering, Located at Central Building Research Institute Roorkee 247667, INDIA,
Tel: 01332- 283464, E-mail: iswe1993@gmail.com,http://www.iswe.co.in
Printed by : *R. K. Printers & Publishers, 26 Civil Lines, New Haridwar Road, Roorkee - 247667 Ph. : 270957, 9897276995*

ISSN : 0973-0613

JOURNAL OF Wind and Engineering

Vol.8 No. 2 July 2011

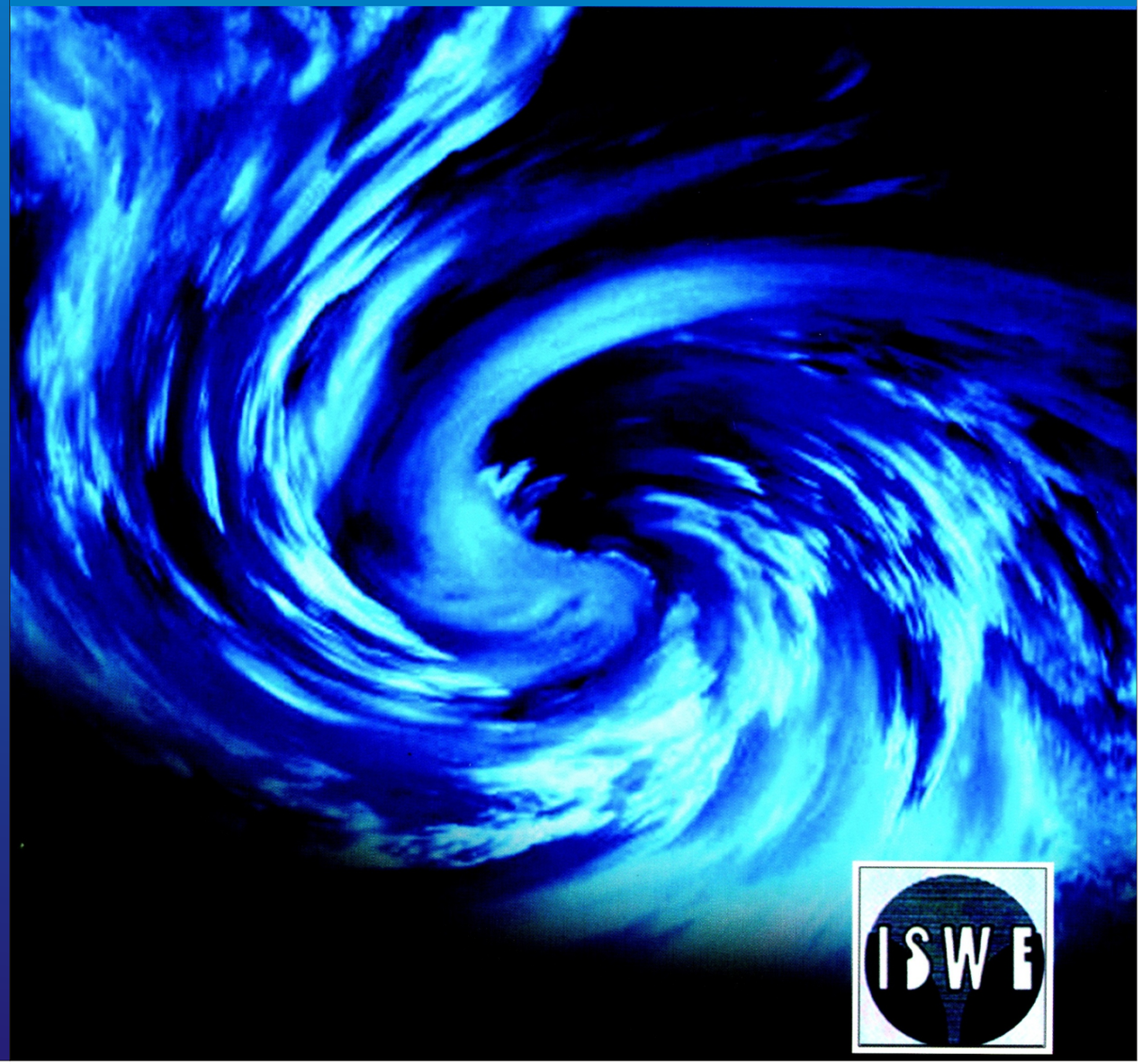

OBJECTIVES OF THE INDIAN SOCIETY FOR WIND ENGINEERING

(a) The Society shall provide a necessary forum to the individuals and institutions connected with, or, interested in industrial aerodynamics, which includes wind effects on structures and buildings, land and sea transportation vehicles; mitigation of disasters due to cyclones, tornadoes, blizzards, sand storms, etc.; wind energy generation; study of atmospheric pollution and dispersion; and, related matters to come together and exchange ideas for the advancement and dissemination of knowledge in the field of Wind Engineering

(b) The Society shall promote research and development work in the field of Wind Engineering and shall maintain close liaison with the International Organizations working with allied objectives.

(c) The Society shall promote research results in professional practice.

(d) The Society shall make efforts to involve field engineers and professional organizations in its activities by arranging seminars, symposia, etc.

(e) The Society shall bring out a periodical publication.

(f) The Society shall institute awards and prizes to recognize excellence of research and application in Wind Engineering.

MEMBERSHIP OF THE SOCIETY

The Society shall have the following categories of membership:

(a) Individual (b) Institutional
(c) Honorary

Subscription: The life membership rates for different categories shall be as follows:

Individual Membership			
Indians and SAARC Nationals	Life	Rs.	2000.00
Other Foreign Nationals	Life	US$	100.00
Institutional Membership	Annual	Rs.	3,000.00
	Regular	Rs.	30,000.00

ISWE EXECUTIVE COMMITTEE

President	Dr. P. D. Porey	Director SVNIT, Surat
Vice-President	Dr. Abhay Gupta	Principal Consultant, ESCOM Noida
Hon. Secretary	Dr. Achal Kumar Mittal	Scientist CBRI, Roorkee
Joint. Seceetary	Dr. P. K. Yadav	STO, CBRI, Roorkee
Treasurer	Dr. Ravi Kumar	Mech. & Ind. Engg. Deptt. IIT Roorkee
Members	Sh. T. N. Gupta	Former Executive Director, BMTPC Delhi
	Dr. (Mrs.) S. Selvi Rajan	Dy Director SERC Chennai
	Dr. (Mrs.) P. Lakshmy	Scientist, CRRI New Delhi
	Sh. Deepak Bansal	Asstt. Chief Projects, HUDCO, Delhi
	Shri. Sanjay Varshney	Asst. Vice President Mahagun India Noida
	Dr. P. Hari Krishan	Scientist. SERC Chennai
	Dr. Y. P. Gupta	Ex-Prof. MNIT Allahabad
	Dr. O. R. Jaiswal Asso.	Prof VNIT, Nagpur
	Dr. Arnab Sarkar	Asst. Prof. IIT Banaras

COMMUNICATION

Communication regarding change of address, subscription renewals, missed numbers, membership and Society Publications should be addressed to -

Dr. Achal Kumar Mittal
Hon. Secretary
Indian Society for Wind Engineering,
Located at the Central Building Research Institute
Roorkee - 247667, INDIA
Tel: 01332- 283464
Mob: +91 9412074408
E-mail: iswe1993@gmail.com, achal_cbri@rediffmail.com
http://www.iswe.co.in

ISSN : 0973 - 0613

JOURNAL OF WIND & ENGINEERING

Vol. 8 No. 2 July 2011

CONTENTS

Journal of wind and Engineering, Vol. 8, No. 2, July 2011, pp. 1-17

Influence factors for wind induced internal pressure in a low rise building with a dominant opening

T.K. Guha[1], R.N. Sharma[1] and P.J. Richards[1]

[1] Department of Mechanical Engineering
University of Auckland, Auckland 1142, New Zealand

ABSTRACT

A covariance integration approach coupled with Eigen value analysis technique is used to determine the influence factors of internal pressure in a low-rise building with a dominant opening. The approach involves determination of the correlated fluctuating external pressure field around the opening as well as the internal pressure fluctuations in order to evaluate the influence factors of fluctuating internal pressure for a range of building volumes, opening sizes and wind speeds tested in the wind tunnel. The results are used to empirically develop non-dimensional design equations of internal pressure influence factors that match the measured data for a normal onset wind flow. Further analysis of influence factors at different angles of wind attack is found to exhibit evidence of oblique flow Helmholtz resonance of internal pressure driven by tangential flow excitation at ±80° for one particular building volume-opening size configuration. The increasing porosity of the building envelope as uniformly distributed background leakage is found to have a damping influence on internal pressure fluctuations associated with a reduction in magnitude of the influence factors.

Keywords **:** Covariance integration; Influence factors; Internal pressure; Design equations; Helmholtz resonance

NOTATION

A_0 Area of opening
l_e Effective length of the air slug
V_0 Nominal building volume
V_e Effective building volume
ρ_a Density of air
P_a Atmospheric pressure
γ Ratio of specific heat capacities
c Opening discharge coefficient
C_L Opening loss coefficient
q Ridge height dynamic pressure
$\overline{U}_h$ Ridge height wind speed
C_{pi} Internal pressure coefficient
$\widetilde{C}_{pi}$ RMS internal pressure coefficient
C_{pe} External pressure coefficient
$\widetilde{C}_{pe}$ RMS external pressure coefficient
f_{hh} Helmholtz frequency
S^* Non-dimensional opening area to building volume ratio
φ_5 Non-dimensional opening area
λ_U Integral length scale of turbulence
t time
t^* Non-dimensional time
C_I Inertia coefficient
a_s speed of sound in air
I_u Turbulence intensity
β^m Mean internal pressure influence factor
β^f Fluctuating internal pressure influence factor
λ Matrix of Eigen value
E Matrix of Eigen vector
$\{\alpha\}$ Vector of modal parameter
n Total number of Eigen modes
g_j Partial energy content

INTRODUCTION

Low and medium rise buildings represent a high percentage of non-engineered or semi-engineered structures, in which internal pressures constitute a major portion of the net wind load across the building envelope. The consideration of appropriate estimates of internal pressure is especially important for designing low rise buildings in cyclone-prone areas where the potential of envelope damage due to debris impact leading to the creation of a dominant opening remains high. The ensuing internal pressure response caused by the breakage of doors and/or windows presents two issues of concern; the internal pressure overshoot, if any, and the dynamic resonant (Helmholtz) response. It is generally accepted that the second of the two issues in combination with high external pressures can generate net load on the envelope or claddings in excess of the design value, thereby resulting in catastrophic failures. A number of wind tunnel studies have corroborated this view and highlighted the need for further strengthening of the quasi-steady based provisions of internal pressure in current wind loading standards. Many of these studies (for e.g. Oh et al., 2007; Sharma and Richards, 2003, 2005) also suggested the possible inadequacies of the current provisions in the wind loading standards such as AS/NZ 1170.2.2002 (2002) to potentially counter such a scenario and proposed suitable remedial measures. The codal committees on the other hand have been somewhat hesitant and on occasions reluctant in implementing their suggestions due to the idealizations involved in these experiments such as the usage of rigid walled building models not representative of real buildings with inherently flexible and leaky envelopes. Many of these early studies (for eg. Sharma and Richards, 2003, 2005) also overlooked the issue of volume scaling necessary to maintain the dynamic similarity between model and full scale such that the chances of occurrence of the vigorous and pronounced Helmholtz resonance reported by them appears questionable in real buildings of any appreciable size and volume. This "difference of opinion" has resulted in an apparent stalemate in which designers continue to use the current wind loading provisions for designing a large number of so-called low rise buildings. The safety of such structures, usually built on modest budget and being unable to afford the high cost of wind tunnel studies, thus depends to a great extent on the suitability of the provisions in the relevant code of practice.

The fact is that both academic literature and the codal provisions pertaining to internal pressures are in general based on "idealized" wind tunnel and full scale studies from a limited range of opening sizes and building volumes. This fails to evoke the confidence necessary for their applicability and usability in typical range of buildings encountered in practice. Hence the need for quantifying the effects of opening sizes and volumes on the provisions of internal pressure is addressed in this paper through presentation of internal pressure influence factors for a range of building volumes, opening sizes and wind speeds obtained from volume-scaled wind tunnel tests. In particular, non-dimensional design equations of influence factors for a normal onset wind flow that agrees well with the experimental data are proposed. Also investigated in some detail is the effect of the angle of wind attack and background leakage on the internal pressure influence factors for differing opening sizes in a building.

The idea of internal pressure influence factors for buildings with openings as presented in this paper is drawn from the conventional dynamic response (such as moments, deflections etc) of structures driven by the fluctuating wind force. Out of a number of methods available for determining the spatial statistics of the fluctuating external pressure that forces the internal pressure response through the opening, the covariance integration method coupled with Eigenvalue analysis as described by Holmes and Best (1981) has been used to determine the influence factors and modal parameters of internal pressures in buildings. The approach involves analyses of the opening external and internal pressure signals obtained from wind tunnel measurements to estimate the internal pressure influence factors with intrinsically incorporated spatial properties of the turbulent flow field.

Journal of wind and Engineering, Vol. 8, No. 2, July 2011, pp. 1-17

THEORETICAL CONSIDERATION

Governing equation of internal pressure with a single dominant opening

The first mathematical treatment of the dynamics of internal pressure in buildings with a dominant opening was presented by Holmes (1979) in his seminal paper in which the internal pressure was conceived of as a response to the wind induced turbulent external pressure fluctuations near the opening. The theory supported by wind tunnel experiments showed that an analogy based on the Helmholtz acoustic resonator can be used to describe the response of internal pressure in a rigid non-porous building (building being treated as a Helmholtz resonator) using a second order non-linear differential equation. Fig. 1 shows a schematic of the proposed model.

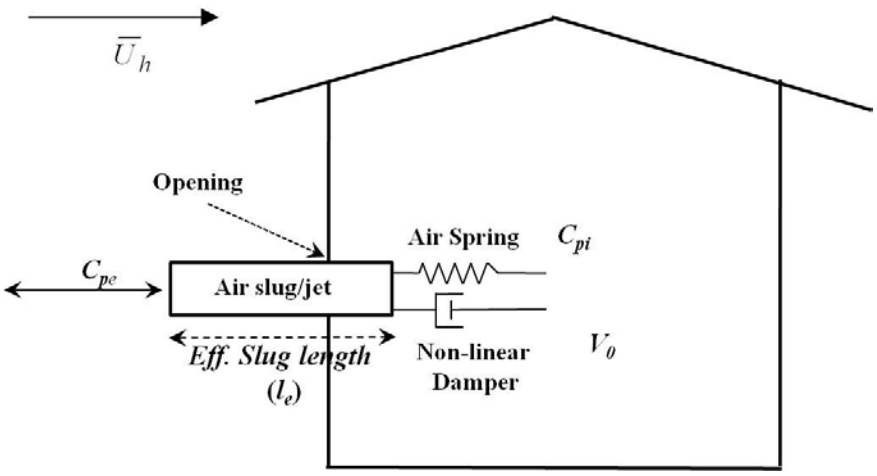

Figure 1. Air slug model (Holmes, 1979)

The derivation assumed a "slug" of air of area A_o and effective length $l_e = \sqrt{\pi A_o / 4}$ to oscillate at the opening under the forcing of external fluctuating pressure, the stiffness being provided by the internal volume (V_o) of air acting as a pneumatic spring and damped by the irrecoverable energy lost due to flow past the opening. Since then, important theoretical contributions from Liu and Saathoff (1981), Vickery and Bloxham (1992), Sharma and Richards (1997), Oh et al. (2007) supported by wind tunnel (Sharma and Richards, 2003, 2005; Oh et al., 2007) and some full scale studies (Ginger et al., 1997; Fahrtash and Liu, 1990; Kwok and Hitchcock, 2009) by others have greatly led to the development of a sound theoretical basis of internal pressure dynamics. A second order ordinary differential equation with
non-linear damping of the form

$$\frac{\rho_a l_e V_e}{\gamma c A_0 P_a}\ddot{C}_{pi} + C_L \frac{\rho_a q V_e^2}{2(\gamma A_0 P_a)^2}\left|\dot{C}_{pi}\right|\dot{C}_{pi} + C_{pi} = C_{pe} \tag{1}$$

has been established by the researchers to model the wind induced internal pressure response of a building cavity with an opening. In this equation, ρ_a is the density of fluid (air in this case) inside the building cavity; V_e is the effective volume of the cavity, being equal to V_0 (the nominal cavity volume) for a building with rigid envelope, and equal to $V_0(1+b)$ for a building with quasi-statically flexible envelope (b being the ratio of the bulk modulus of air inside the cavity to that of the building envelope); $\gamma = 1.4$ is the ratio of specific heat capacities; P_a is the ambient pressure of air; c and C_L are the discharge and loss coefficients of flow through the opening;

$q = 0.5\rho_a \overline{U}_h^2$ is the ridge height dynamic pressure for a ridge height velocity of $\overline{U}_h$; and $C_{pi} = p_i/q$ and $C_{pe} = p_e/q$ are the internal and external pressure co-efficient respectively. It is worth noting that significant differences still exist in the values for the ill-defined parameters (c, C_L and l_e).
The undamped resonant frequency (also known as the Helmholtz frequency) is given by,

$$f_{hh} = \frac{1}{2\pi}\sqrt{\frac{\gamma c A_0 P_a}{\rho_a l_e V_0}} \tag{2}$$

Equation (1) implies that under favourable forcing by the external pressure (i.e. with enough turbulence energy) near the opening, the internal pressure can exhibit a significant resonating response at the Helmholtz frequency (given by Equation 2) of the cavity-opening combination much like the dynamic response of a structure under the fluctuating wind load. While the strongest resonance of internal pressure due to turbulent buffeting is expected for an onset flow normal to the opening, Sharma and Richards (2003) have shown using wind tunnel tests that an even stronger resonance of internal pressure driven by "eddy dynamics" is possible at an oblique flow angle under certain conditions, of the reduced frequency of internal volume and opening size. This is irrespective of whether or not, the Helmholtz frequency of the building-opening combination lies in the energy containing region of the turbulent velocity spectrum. Thus, at the condition of a resonating internal pressure driven by turbulent buffeting or "eddy dynamics", the net dynamic load on the building envelope as a whole, or in parts (such as claddings), may increase considerably leading to its failure.

Non-dimensional form of the governing equation

A non-dimensional form of the governing equation of internal pressure given by Equation (1) was proposed by Holmes (1979) by introducing non-dimensional parameters S^* [$=\left(A_0^{3/2}/V_e\right)\left(a_s/\overline{U}_h\right)^2$, where a_s is the speed of sound] and φ_5 [$=\lambda_U/\sqrt{A_0}$, λ_U is the integral length scale of turbulence at the building ridge height] and a non-dimensional time as t^* [$=t\overline{U}_h/\lambda_U$]

$$\frac{C_I}{cS_*\phi_5^2}\frac{d^2C_{pi}}{dt_*^2} + \frac{C_L}{4\left(S_*\phi_5\right)^2}\left|\frac{dC_{pi}}{dt_*}\right|\frac{dC_{pi}}{dt_*} + C_{pi} = C_{pe} \tag{3}$$

In the equation, C_I is the inertia coefficient of flow through the opening. Equation (3) shows that a unique solution of internal pressure variation forced by the external pressure fluctuations (C_{pe}) for a given value of c, C_I, C_L, S^* and φ_5 is possible and can be represented by a family of curves of the fluctuating internal pressure (Ginger et al., 2008) as function of variables S^* and φ_5.

Design equations

Holmes and Ginger (2009) non-dimensionalised the expression for the ratio of standard deviations of internal ($\widetilde{C}_{pi}$) and external pressure ($\widetilde{C}_{pe}$) coefficient fluctuations developed by Vickery and Bloxham (1992) under the approximation of external pressure as a 'white noise' inducing internal pressures with a dominant resonant contribution in comparison to the low frequency 'background' noise. The formula derived using a Von-Karman spectral density for the external pressure forcing by introducing $\widetilde{C}_{pe} = 0.35$, $C_I = \sqrt{\pi/4}$ and an empirical term $\alpha_c = 1.5$ (for large volumes) is given as

Journal of wind and Engineering, Vol. 8, No. 2, July 2011, pp. 1-17

$$\frac{\tilde{C}_{pi}}{\tilde{C}_{pe}} = \left[\left(1 - \frac{0.564}{\left\{ S^* \phi_5^2 \right\}^{1/3}} \right) + 2.41 \left(\frac{S^*}{C_L^{3/2} \phi_5} \right)^{4/9} \right]^{1/2} \tag{4}$$

An alternative expression for the ratio of internal to external pressure fluctuations was derived by RWDI (1993) by neglecting the inertial term in Equation (3) as

$$\frac{\tilde{C}_{pi}}{\tilde{C}_{pe}} = \frac{1}{\sqrt{\sqrt{C_L} \frac{\lambda_U}{10 \overline{U}_h S^* \phi_5} + 1}} \tag{5}$$

This was later adopted by American Loading Standard ASCE 7-05 (2005) by further simplifying Equation (5) through assumption of the following values of the parameters; $C_L = 44.44$, $\overline{U}_h$=25m/s, a_s=340m/s, λ_U =100m.

$$\frac{\tilde{C}_{pi}}{\tilde{C}_{pe}} = \frac{1}{\sqrt{1 + \frac{1}{6936} \frac{V_0}{A_0}}} \tag{6}$$

A performance evaluation carried out by Holmes and Ginger (2010) using both the analytical models, Equations (4) and (5), with their experimental data resulted in the Vickery and Bloxham model overpredicting the internal pressure fluctuations beyond S^* of about 10 due to an overestimation of the resonant component and underprediction by the RWDI model, due to neglecting the inertial term, at all but very small values of S^*. The ACSE version of the model was found to give even lower predictions compared to the RWDI version due to its usage of a higher C_L value. An alternate bi-linear model derived empirically by fitting the measured data was proposed as

$$\frac{\tilde{C}_{pi}}{\tilde{C}_{pe}} = 1.1 + \left(\frac{4}{\phi_5} \right) \log_{10}\left(S^* \right) \qquad \text{for } 0.1 < S^* < 1.0 \tag{7a}$$

$$\frac{\tilde{C}_{pi}}{\tilde{C}_{pe}} = 1.1 \qquad \text{for } S^* > 1.0 \tag{7b}$$

For internal pressure fluctuations generated by atmospheric turbulence as is the case for a normal onset turbulent flow, Holmes and Ginger (2010) have shown that the internal pressure gust factor (γ_i) and the ratio of the peak internal to external pressures can be determined from:

$$\gamma_i = 1 + 2 g I_u \left(\frac{\tilde{C}_{pi}}{\tilde{C}_{pe}} \right) \tag{8a}$$

$$\frac{\hat{C}_{pi}}{\hat{C}_{pe}} = \frac{1 + 2 g I_u \left(\frac{\tilde{C}_{pi}}{\tilde{C}_{pe}} \right)}{1 + 2 g I_u} \tag{8b}$$

where g is the peak factor (3.5 to 4) and I_u is the intensity of turbulence. The ratio of the internal to external pressure fluctuations needed in the estimation of Equation (8) can be obtained from Equations (4), (5), (6) or (7).

COVARIANCE INTEGRATION METHOD AND EIGENVALUE ANALYSIS

As mentioned earlier, a different analysis technique namely the covariance integration approach has been used in the current study to generate influence factors for a range of opening sizes, volumes and wind speeds subjected to wind tunnel tests. The influence factors, which are a measure of the ratio of the internal to external pressure fluctuations weighted over the tributary areas that make up the opening, are presented in Equation (7), a non-dimensional format similar to that reported by Holmes and Ginger (2010).

It is assumed for the purpose of this analysis that the pressures acting on the surface of the building around the opening are stationary, ergodic random processes. This will be close to reality when the mean velocity ($\overline{U}_h$) can be assumed to be nearly constant over the period of the passage of storms. Assuming equal loss coefficient over all the tributary areas, the mean internal pressure $\overline{p}_i$ influenced by mean external pressure $\overline{p}_{e_j}$ acting over an opening tributary area A_j with a mean influence factor β_j^m is given by

$$\overline{p}_i = \frac{\sum_{j=1}^{n} A_j^2 \beta_j^m \overline{p}_{e_j}}{\sum_{j=1}^{n} A_j^2} \tag{9}$$

where n is the number of tributary areas representing the external pressure taps around the opening influencing the internal pressure. If $A_j = A_k \left(j \neq k\right)$, then Equation (9) reduces to

$$\overline{p}_i = \frac{\sum_{j=1}^{n} \beta_j^m \overline{p}_{e_j}}{n} \tag{10}$$

Similarly the root mean square fluctuating internal pressure ($\widetilde{p}_i$) can be shown to be influenced by the fluctuating external pressures acting on tributary areas over the opening as

$$\widetilde{p}_i = \left(\overline{p_i'^2}\right)^{1/2} = \left(\frac{\sum_{j=1}^{n}\sum_{k=1}^{n} A_j A_k \beta_j^f \beta_k^f \overline{p'_{e_j} p'_{e_k}}}{\sum_{j=1}^{n}\sum_{k=1}^{n} A_j A_k} \right)^{1/2} \tag{11}$$

where β_j^f and β_k^f are fluctuating influence factors for tributary areas A_j and A_k respectively. Normalized by the ridge height dynamic pressure *q*, Equation (11) can be expressed in coefficient form as

$$\widetilde{C}_{pi} = \left(\frac{\sum_{j=1}^{n}\sum_{k=1}^{n} A_j A_k \beta_j^f \beta_k^f r_{jk} \widetilde{C}_{pe_j} \widetilde{C}_{pe_k}}{\sum_{j=1}^{n}\sum_{k=1}^{n} A_j A_k} \right)^{1/2} \tag{12}$$

where r_{jk} is the correlation coefficient between the fluctuating pressures at areas A_j and A_k and $\widetilde{C}_{pi}$ is the root mean square (RMS) value of fluctuating internal pressure. Assuming $A_j = A_k \left(j \neq k\right)$ and restating Equation (12) in matrix form results in

Journal of wind and Engineering, Vol. 8, No. 2, July 2011, pp. 1-17

$$\widetilde{C}_{pi}=\left(\frac{\{\beta^f\}^T[A][\widetilde{C}_{pe}][r][\widetilde{C}_{pe}][A]\{\beta^f\}}{n^2[A]^2}\right)^{1/2}=\frac{1}{n}\left(\{\beta^f\}^T[\widetilde{C}_{pe}][r][\widetilde{C}_{pe}]\{\beta^f\}\right)^{1/2} \tag{13}$$

where the RMS external pressure coefficient diagonal matrix [$\widetilde{C}_{pe}$] and the correlation coefficient matrix [r], both of order n can be combined together to form the pressure coefficient covariance matrix ([C_p]) as

$$[C_p]=[\widetilde{C}_{pe}][r][\widetilde{C}_{pe}] \tag{14}$$

The pressure coefficient covariance matrix [C_p] and the RMS internal pressure coefficient are evaluated from the sampled pressure signals, around the opening and inside the cavity respectively, in the wind tunnel. Further, if it is assumed that the influence factors $\beta_j^f,(j=1:n)$ of the fluctuating internal pressure due to the external pressure acting over each tributary area are equal, then an expression for the fluctuating internal pressure influence factor for a particular angle of wind attack $\beta_j^f(\theta)$ can be derived as

$$\beta^f(\theta)=\frac{n\widetilde{C}_{pi}}{\sqrt{\sum_{j=1}^{n}\sum_{k=1}^{n}C_{p_{jk}}}} \tag{15}$$

Eigenvalue analysis or Proper Orthogonal Decomposition (POD) can be applied to the pressure coefficient covariance matrix [C_p] given by Equation (14) such that the Eigenvalues $\lambda_j(j=1:n)$ sorted in order of magnitude can be arranged into a n^{th} order diagonal matrix $[\lambda]$. This along with the corresponding matrix of normalized Eigenvectors $[E]$ can be used for reduction into the diagonal form as

$$[\lambda]=[E]^{-1}[C_p][E] \tag{16}$$

A vector of modal parameter $\{\alpha\}$ can be defined (Best and Holmes, 1981) as

$$\{\alpha\}=[E]^{-1}\{\beta\}=[E]^T\{\beta\} \tag{17}$$

can be used to investigate the relative contribution of the individual modes to internal pressure dynamics. The RMS internal pressure coefficient ($\widetilde{C}_{pi}$) can be re-generated using Equations (13), (16) and (17) using all (n) or a small number ($n_s \leq n$) of dominant Eigenmodes associated with large Eigenvalues

$$\widetilde{C}_{pi}=\frac{1}{n}\sqrt{\{\alpha\}^T[E]^T[C_p][E]\{\alpha\}}=\frac{1}{n}\sqrt{\{\alpha\}^T[\lambda]\{\alpha\}}\cong\frac{1}{n}\sqrt{\sum_{j=1}^{n_s\leq n}\alpha_j^2\lambda_j} \tag{18}$$

A metric for exhibiting the relative modal contributions of the fluctuating external flow field to internal pressure fluctuations can be established in terms of the partial energy content (g) of each participating mode although other more complicated criteria can be set up as well (Liang et al., 2006). The value of g is calculated as

$$g_j=\frac{\lambda_j}{\sum_{j=1}^{n}\lambda_j}\times 100 \tag{19}$$

is used to justify the assumption of equal influence factors due to each tributary opening area in the current analysis.

EXPERIMENTAL DETAILS

Boundary layer simulation

A 1:100 scale boundary layer profile approximately representing terrain category 3 as per AS/NZS 1170.2.2002 (2002) was simulated in the 11m long by 1.8m wide by adjustable 1.2m high low speed section of the De' Bray's boundary layer wind tunnel at the University of Auckland. A combination of turbulence generators including log spaced grill, vertical spires, saw tooth barrier, floor blocks and 10-20mm average sized gravels was used to generate the boundary layer flow. The mean velocity and turbulence intensity profiles of the simulated terrain at the test section centre and at a location 600mm upstream are shown in Fig. 2(a) and (b) along with the codal provisions. While the simulated non-dimensionalised mean velocity profile show a reasonable agreement with the codal provisions, the turbulence intensity of the boundary layer simulated in the wind tunnel tends to be lower than the codal specifications. The shear velocity (u_*) and the simulated roughness (z_o) height calculated from the velocity profile are 0.72m/s and 0.23m respectively in full scale. Fig. 2(c) shows the non-dimensionalised longitudinal velocity spectra measured at the ridge height of the building along with the fitted Von Karman spectrum. The measured integral length scale of 0.248m in the wind tunnel (equivalent to 24.8m in full scale) at the building ridge height is found to be much lower than its target value of 54m due to the constraints posed by the tunnel walls.

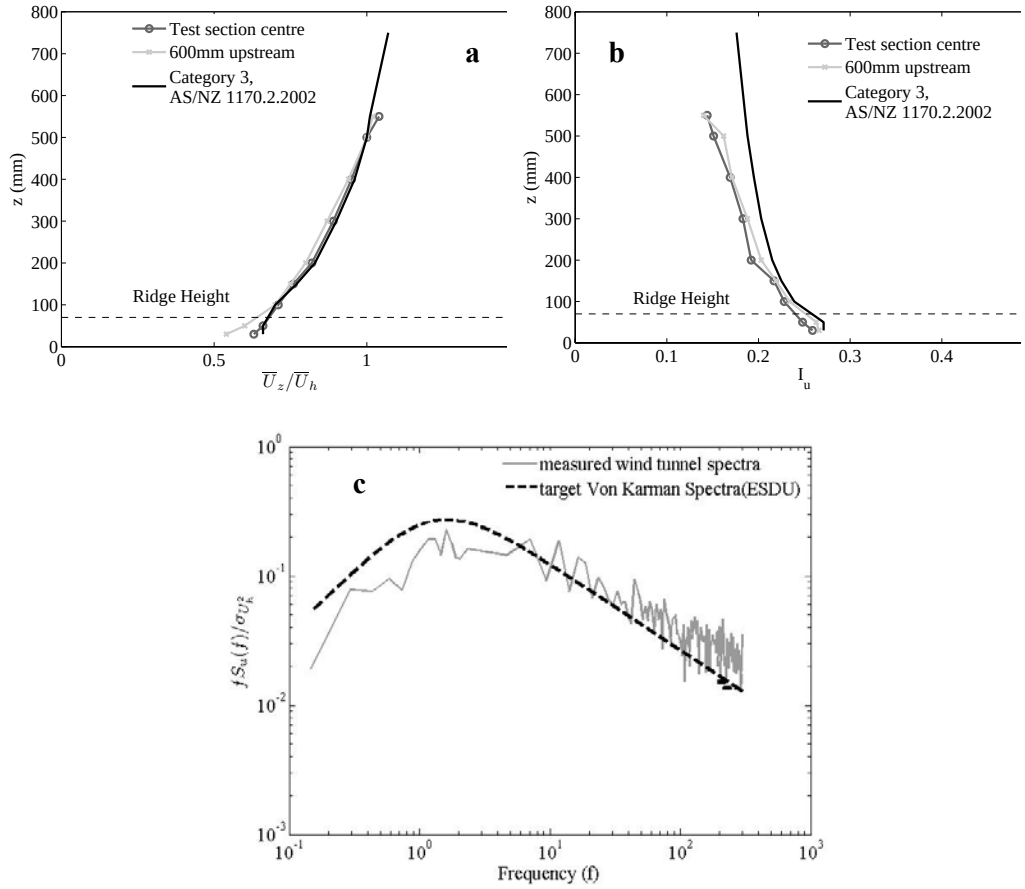

Figure 2. Simulated boundary layer characteristics (a) velocity (b) turbulence intensity and (c) spectrum of longitudinal turbulence

Journal of wind and Engineering, Vol. 8, No. 2, July 2011, pp. 1-17

Model details

The Twisted Flow Wind Tunnel (TFWT) building of the University of Auckland, the basic model of which is used for wind tunnel investigations, is a typical warehouse consisting of a large hall housing the Twisted Flow Wind Tunnel with adjoining office space. It is located on the outskirts of the Auckland city in an industrial area at Tamaki flanked by similar structures to its north and the west. The hall of dimensions 35.1m by 24.9m by 7m consists of a roller door of size 5m by 4.2m in its southern wall that opens into a space interspersed with obstructions such as bushes, fences, cargo containers not more than 5 m high. The setting, suburban in nature is representative of a category 3 terrain profile as per AS/NZS 1170.2.2002 (2002).

The aerodynamic information including records of internal pressure and external pressure around the opening are obtained from wind tunnel tests using a 1:100 scale model of the TFWT building of The University of Auckland at Tamaki. Since the purpose of this study was to accurately simulate the dynamic internal pressure response of the hall with a large door opening, care was taken to model the internal volume cavity for a ridge height velocity ratio (model to full scale) of 1:4 by way of internal volume scaling below the wind tunnel floor. This was achieved by exaggerating the internal volume of the hall cavity of dimensions 351mm by 249mm by 70mm using a sealed plywood chamber 322mm by 322mm by 795mm hanging from the turntable below the tunnel floor as shown in Fig. 3(a). In addition, the roof and the leeward wall consisted of 70 uniformly distributed leakage holes, of 2.5mm diameter each, for a porosity ratio (Total area of leakages/Total wall area including the roof) of 0.2%. The leakages could be sealed off in any combination to alter the building porosity.

A total of 64 channels of pressure data including 51 external taps distributed evenly on the face containing the opening, 4 external taps each on the roof and the opposite face, 4 internal taps in the hall cavity, 1 internal tap in the adjoining office space and 1 channel for dynamic pressure were sampled simultaneously at 600Hz for 120 seconds for different wind angles [θ in Fig. 3(a)] varying from 0 to 360° in 20° increments. Out of the 51 external pressure taps on the face containing the opening of dimensions 5cm by 4.2cm, a total of 11 taps [marked as black cross in Fig. 3(b)], each representing the pressure over a single tributary opening area, were evenly distributed around the opening at equal distance from each other. The pressure signals transmitted to the module housing the differential transducers (range ~± 650 Pa, XSCL series, Honeywell Inc.) through 550mm long PVC tubes of 1.5mm internal diameter were subsequently corrected for tubing induced distortion using a time-domain based recursive filter approach (Halkyard et al., 2009). Care was taken to seal off the hole as much as possible, through which the pressure tubings were carried outside to the transducer module, using special air-tight sealants and tapes. The internal volume modified by the tubings was found to be less than 0.1%, and hence is assumed to have a negligible effect on the internal pressure dynamics. The transducers along with the signal conditioning equipment was interfaced to a PC equipped with a data logging program written in LABVIEW program through a multiplexer and a 16 (analog) channel DAQ card (USB 6211, National Instruments Inc.). The transducers were referenced to the static pressure measured using a pitot tube placed 500mm (50m in full scale) above the wind tunnel floor approximately 12 building heights upstream of the model. The total pressure also measured simultaneously using the same Pitot tube was used to obtain the dynamic pressure (hence velocity) at that height. A frequency dependant transfer function established from a different set of hotwire tests involving simultaneous velocity measurements at the reference (500mm) and the building ridge height (70mm) at the test section without the model was used to convert the mean and fluctuating velocity at the reference height to that at the building ridge height.

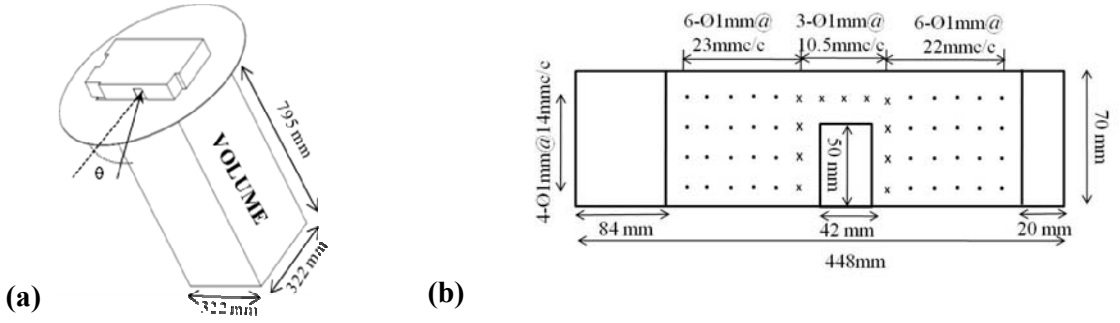

Figure 3. (a) Schematic of the wind tunnel model along with volume scaling and (b) Layout of external pressure taps on the windward wall with the opening (All dimensions in mm)

A number of model configurations involving a range of building volumes, opening sizes, wind speeds and angle of attack were tested in the wind tunnel. While the opening sizes (hence φ_5) were altered using acrylic plugs of various size, the overall volume of the model (and hence S^*) was varied using polystyrene (foam) blocks of different dimensions. Table 1 summarizes the different designations of building volumes, opening sizes, wind speeds and their magnitudes used in the study.

Table 1. Model configurations tested in the wind tunnel

Volume designation	V_0	V_{15}	V_{30}	V_{45}	V_{60}	V_{93}
Magnitude(m^3)	0.089	0.075	0.062	0.049	0.035	0.006

Opening size designation	A_{100}	A_{80}	A_{50}	A_{30}	A_0
Magnitude (m^2)	0.002	0.0017	0.001	0.0006	0.0

Ridge height wind speed designati	W_{60}	W_{65}	W_{70}	W_{75}	W_{80}
Magnitude (m/s)	5.7	6.2	6.7	7.2	7.6

Table 2 summarizes the different permutation-combinations of the parameters used to present the influence factors in this paper.

Table 2. Combinations used in the current work

Building Volume	Opening size	Angle of attack (θ	Leakage	Wind speed
V_0	$A_0;A_{30};A_{50};A_{80};A_{10}$	0:20:360	No/Yes	W_{65}
		0	No	$W_{60};W_{65};W_{70};W_{75};W_{80}$
V_{15}	$A_{30};A_{50};A_{80};A_{100}$	0	No	$W_{60};W_{65};W_{70};W_{75};W_{80}$
V_{30}	$A_{30};A_{50};A_{80};A_{100}$	0	No	$W_{60};W_{65};W_{70};W_{75};W_{80}$
V_{45}	$A_{30};A_{50};A_{80};A_{100}$	0	No	$W_{60};W_{65};W_{70};W_{75};W_{80}$
V_{60}	$A_{30};A_{50};A_{80};A_{100}$	0	No	$W_{60};W_{65};W_{70};W_{75};W_{80}$
V_{93}	$A_{30};A_{50};A_{80};A_{100}$	0	No	$W_{60};W_{65};W_{70};W_{75};W_{80}$

Journal of wind and Engineering, Vol. 8, No. 2, July 2011, pp. 1-17

RESULTS AND DISCUSSION

Effect of opening size

Influence factors for fluctuating internal pressure calculated using Equation (15) for volume V_0 and a ridge height wind speed of 6.2m/s (W_{65}) are plotted in Fig. 4 for the different opening sizes listed in Table 2. The influence factors for internal pressure are found to vary significantly with the size of the opening. In fact the influence factors for A_{100} are consistently 4-5 times higher for the windward angles and around 2-3 times higher than for sidewall and leeward angles in comparison to those for A_0 configuration; implying that the size of the opening, over which the external pressure acts, is an important factor influencing the internal pressure fluctuations as theoretically predicted.

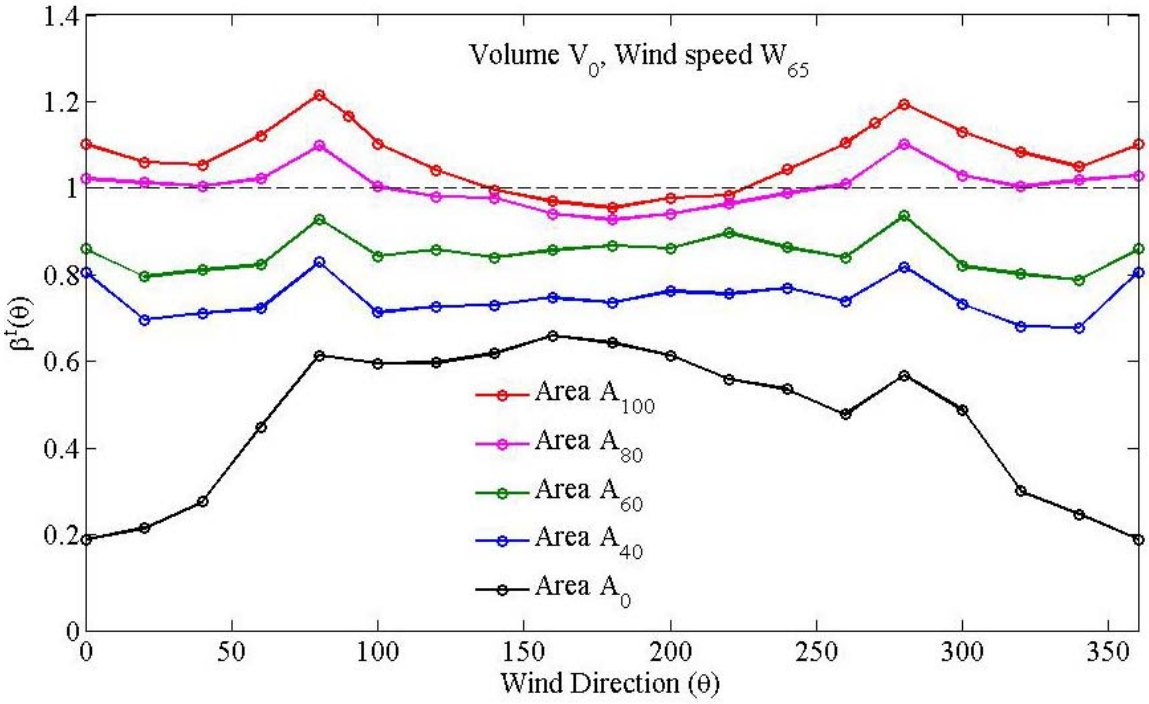

Figure 4. Influence coefficient for a building with volume V_0 and different opening size at wind speed W_{65} in the wind tunnel

While the influence factor for A_{100} and A_{80} configurations at all wind directions, except leeward openings, is in excess of unity, most prominent effects of increased internal pressure fluctuations are visible at around ±80:90° for all configurations. This increased fluctuation of internal pressure in comparison to the external pressures is attributed to the resonant effects. This is further demonstrated in Fig. 5 which shows the admittance function of fluctuating internal pressure over the averaged external pressure at these angles of wind attack (θ). Higher gains of internal pressure at the frequency of 33Hz, corresponding to the theoretical Helmholtz frequency given by Equation (2), are attributed to the Helmholtz resonance. At these wind angles corresponding to the sidewall opening situations, oblique flow resonance of internal pressure due to "eddy dynamics" or tangential flow excitation as reported by Sharma and Richards (2003) is believed to have contributed to this observation.

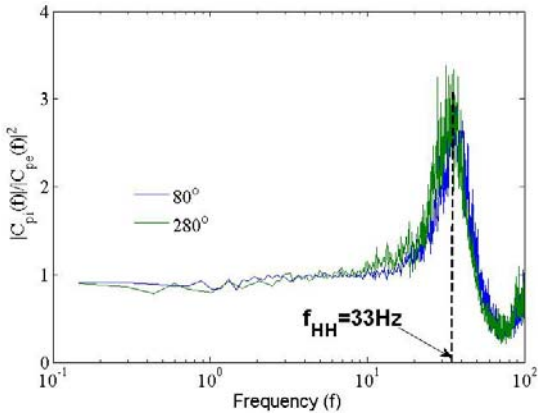

Figure 5. Frequency dependant gain of internal over external pressure

Effect of background leakage

Typical porosity (defined as the ratio of the leakage to the wall area) of modern buildings in Australia/New Zealand range from 0.01% to 0.2%. In the context of the current analysis, porosity ratio is defined as the ratio of the leakage to the dominant opening area. Representative leakages of 10% and 20% uniformly distributed on roof and the leeward wall were used to determine its effect on the fluctuating internal pressure influence factors induced through a dominant opening inside the building. Such porosity ratios are usually considered conservative from a design point of view (Vickery and Bloxham, 1992; Oh et al., 2007). Fig. 6 plots the influence factors for the building V_0 with opening A_0 with and without background leakage.

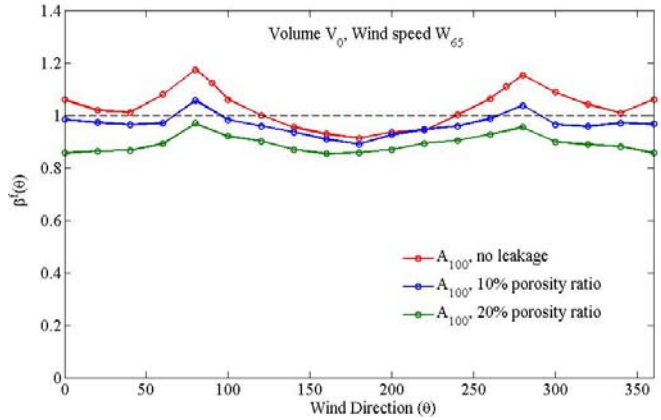

Figure 6. Effect of background leakage (porosity) on the influence factors of internal pressure of a building with a dominant opening

The effect of background leakage on fluctuating internal pressure is evident from the reduction in magnitude of the influence factors with increase in building porosity. In other words, the influence of the external pressure around the dominant opening as well the resonant response of the building cavity in determining the magnitude of internal pressure fluctuations is reduced by the damping effect of background leakages. A detailed theoretical and experimental investigation of the effect of background leakage on the dynamic internal pressure has been reported by Yu et al. (2008).

Proper Orthogonal Decomposition (POD)

In order to estimate the relative contribution of the different modes of the fluctuating external pressure around the opening to internal pressure fluctuations, modal parameter α and the partial energy content (g) calculated, as per Equations (17) and (19) respectively, for wind directions, 0° and ±80° are plotted in Fig. 7(a) and 7(b) for

Journal of wind and Engineering, Vol. 8, No. 2, July 2011, pp. 1-17

building V_0 with opening area A_{100}. These wind directions were chosen due to the relatively higher values of influence coefficient β^f obtained at these angles in Figure 4.

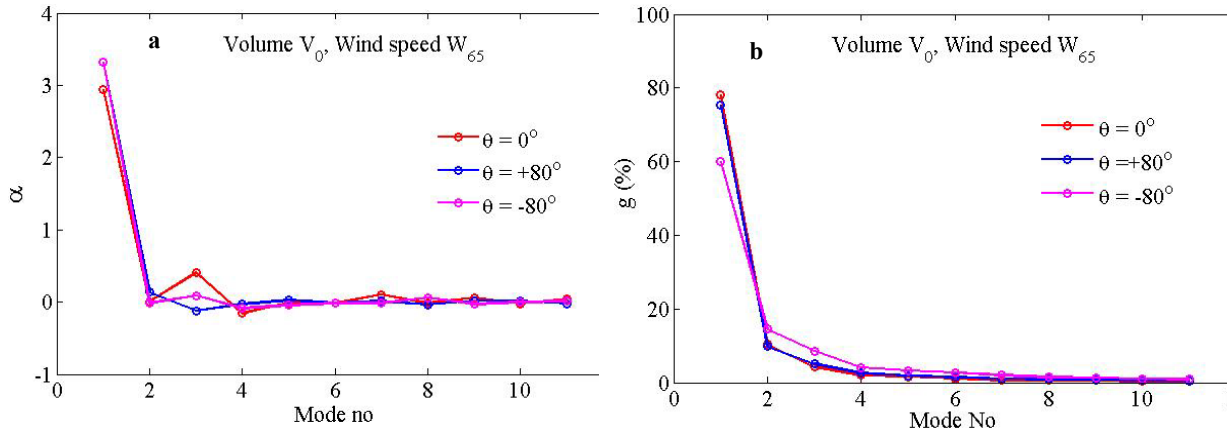

Figure 7. Magnitude of the (a) modal parameter, α and (b) partial energy content, g of the participating modes for building volume V_0 with opening A_{100} at different angles of wind attack

The first modal parameter α for any given wind directions is much higher in magnitude compared to others in Figure 7(a) and hence will provide maximum contribution to internal pressure fluctuations. The first mode can be seen in Figure 7(b) to contribute around 75-80% of the fluctuating energy, reconstruction (n_s=1) using which would generate a fluctuating pressure field around the opening, accurate enough for engineering purpose.

The first fluctuating mode of external pressure around the opening can be considered to represent low frequency turbulence in the flow field, induced by eddies of size equal to the integral length scale of turbulence at the opening height of the building for a windward opening case. These eddies, usually much larger than the opening dimensions, induce highly correlated external pressures over the opening area. This somewhat justifies the consideration of equal contribution of external pressure over a tributary opening area (represented by an external pressure tap) to internal pressure fluctuations in the estimation of influence factors.

Design solutions

Often the critical design case, particularly during severe storm events is the case with a single windward dominant opening either created accidently, produced by the impact of wind borne debris or by direct wind loading. Quantification of the influence factors of internal pressure in such situations has been carried out for a range of building volumes, opening area and wind speeds listed in Table 2.

Fig. 8 plots the internal pressure influence coefficients obtained in the current study as a function of S^* for different opening sizes (i.e. φ_5) in comparison with the RMS internal to external pressure ratios predicted by non-dimensionalized Vickery and Bloxham (V&B) model (Eq. 4), RWDI (I&D) model (Eq. 5) and Holmes and Ginger (H&G) model (Eq. 7). A loss coefficient of C_L=2.78 (corresponding to k = 0.6 as per Holmes models) is used for analysis along with the integral length scale values of 24.8m (full scale) for the Category 3 terrain measured in the wind tunnel.

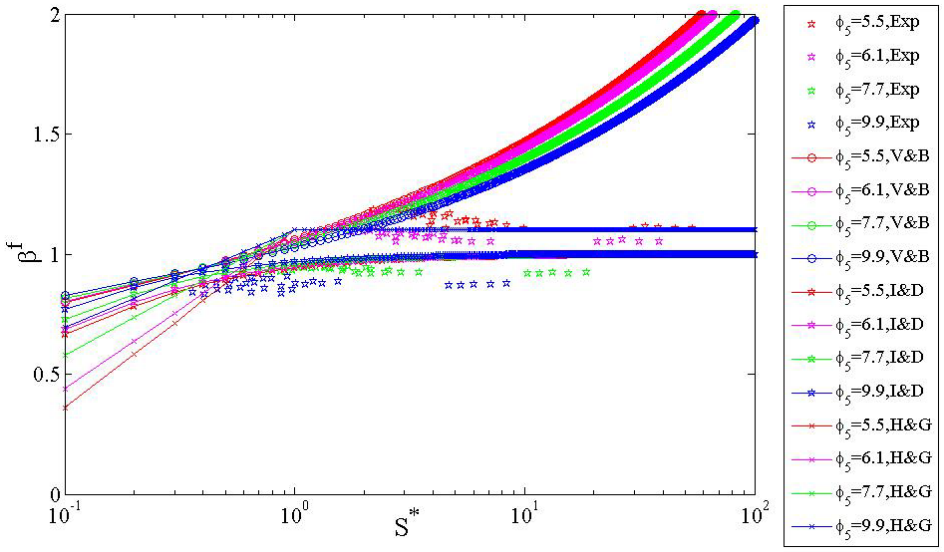

Figure 8. Comparison of Vickery and Bloxham (V&B), RWDI (I&D) and Holmes and Ginger (H&G) model with experimental data for internal pressure influence factors (β^f)

The V&B model in general, appears to be conservative for all but lower values of S^* corresponding to ϕ_5=5.5 (A_{100}) whereas the I&D model appears to under predict the measured values at higher S^* for larger openings (ϕ_5=5.5 and 6.1). H&G model on the other hand provides safe design values for all but a small range of S^* between 2 and 6 for the largest opening configuration (ϕ_5=5.5).

Interestingly, none of these models exhibit such a high sensitivity to area size (or ϕ_5) as observed in the current experiments. This makes all the models highly conservative, especially for smaller opening sizes (ϕ_5=7.7 and 9.9 in the current study), across all values of S^*. This is possibly due to the location of these smaller openings away from the stagnation region with high external pressures. The locations of the openings on the windward wall used in the current study are illustrated in Figure 9 along with the relevant dimensions.

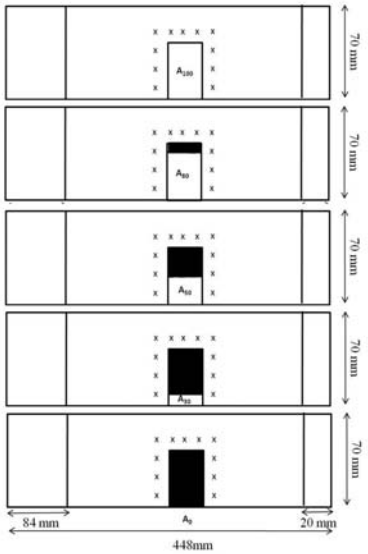

Configuration	Height (mm	Width (mm
A_0	0	42
A_{30}	15	42
A_{50}	25	42
A_{80}	40	42
A_{100}	50	42

Figure 9. Opening configurations (size and location) studied in the wind tunnel (figure not to scale)

Journal of wind and Engineering, Vol. 8, No. 2, July 2011, pp. 1-17

Hence to match the current dataset, a modified set of equations sensitive to the opening location is proposed

$$\beta^f = \frac{\phi_5^2}{55} - \frac{\phi_5}{2.9} + 2.51 + \left(\frac{1}{\phi_5}\right)\log_{10}\left(S^*\right) \quad \text{for } 0.1 < S^* < 1.0 \tag{20a}$$

$$\beta^f = \frac{\phi_5^2}{55} - \frac{\phi_5}{2.9} + 2.51 \qquad \text{for } S^* \geq 1.0 \tag{20b}$$

Fig. 10 provides a comparison of the proposed model with the experimentally obtained influence factors and shows the required sensitivity of the dynamic internal pressure to area size and location of the opening in the wall.

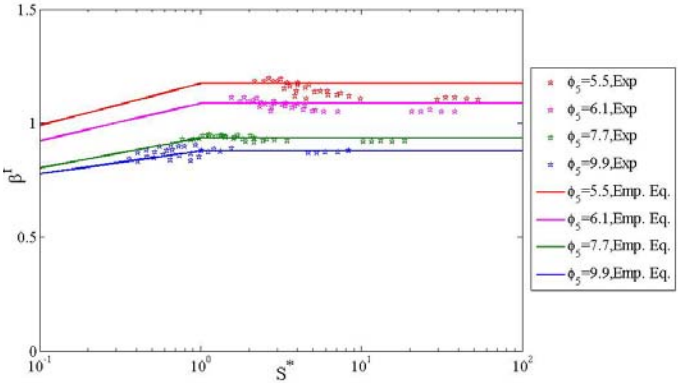

Figure 10. Comparison of the predicted and experimentally obtained influence factors (β^f)

Equation (20a and 20b) can be further simplified for implementation in wind loading standards using hard-coded values of ridge height wind speed ($\overline{U}_h$=25m/s), loss factor (C_L=44) and integral length scale (λ_U =25m) as was done by RWDI (1993) or by Holmes and Ginger (2009) leading to

$$\beta^f = \frac{11.4}{A_0} - \frac{8.6}{\sqrt{A_0}} + 2.51 + 0.04\sqrt{A_0}\log_{10}\left(185\frac{A_0^{3/2}}{V_0}\right) \quad \text{for } \frac{1}{1850} < \frac{A_0^{3/2}}{V_e} < \frac{1}{185} \tag{21a}$$

$$\beta^f = \frac{11.4}{A_0} - \frac{8.6}{\sqrt{A_0}} + 2.51 \qquad \text{for } \frac{A_0^{3/2}}{V_e} \geq \frac{1}{185} \tag{21b}$$

but can be suitably modified using specific parameters for a site/region either obtained from field tests or through consultation of relevant wind loading standards of the region/country, ESDU (2001) and ASHRAE (2001) guidelines.

Fig. 11 plots the Lieblein BLUE (1974) fitted peak ratio of fluctuating internal to opening external pressures measured in the wind tunnel in comparison to the peak ratio predicted by the empirical model (Eq. 20) in conjunction with Eq. 8(b). Lieblein analysis involved dividing the sampled data into twenty equal segments, weighting the sorted peak values of each of the segments using BLUE estimators to calculate the mode and dispersion of the Type I extreme value distribution and using them to determine the mean ½ hour (full scale) peak pressure coefficient values. The Lieblein peaks are slightly lower than the recorded worst peak pressure coefficients in the study but are considered to be statistically more reliable.

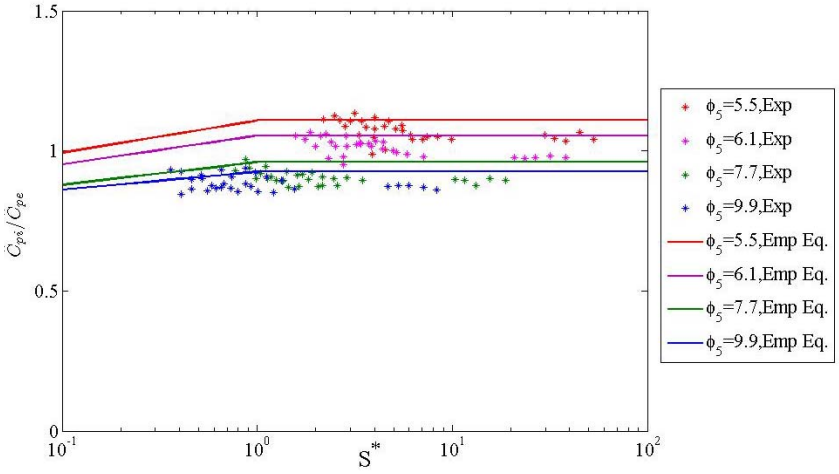

Figure 11. Comparison of the predicted and the measured peak ratio of internal to external pressure The agreement between the predictive model and the measured data is found to be satisfactory.

CONCLUSION

Influence factors of fluctuating internal pressure are evaluated for a range of building volumes, opening sizes and wind speeds tested in the wind tunnel at different angles of attack using the covariance integration approach. The results are used to empirically develop non-dimensional design equations of influence factors for a normal onset wind flow for category 3 terrain roughness condition based on data-fit. The ratios of the peak internal to external pressures are also found to be predicted satisfactorily by the presented model. In particular, the sensitivity of influence factors to the size and location of the opening in the wall, evident in experiments, are accounted for in the model.

Investigations of the effect of opening area on the influence factors at different wind angles showed that, for a building with an opening near the stagnation zone i.e. at around two-third of the building height, influence factors are approximately 4-5 times higher for the windward angles and around 2-3 times higher for sidewall and leeward angles, compared to that of a sealed building. Maximum value of influence factors, in excess of unity, observed at wind angles of ±80:90° for the building are believed to be due to internal pressure resonance driven by “eddy dynamics” due to tangential flow excitation. The increasing porosity of the building envelope present as uniformly distributed background leakage is found to have a damping influence on internal pressure fluctuations associated with a reduction in magnitude of the influence factors.

Eigenvalue analysis of the opening external pressure covariance matrix, corresponding to wind angles with high influence factors, indicates that 75-80% of internal pressure fluctuations are contributed by the first mode while the contributions of higher modes are less significant. This observation is used to justify the consideration of equal contribution of external to internal pressure fluctuations due to each tributary opening area in the evaluation of influence factors.

REFERENCES

1. American Society of Civil Engineers Standard. Minimum design loads for buildings and other structures. ACSE/SEI 7-05, New York, 2006.
2. ASHRAE. ASHRAE Handbook: Fundamentals, SI ed. American Society of Heating, Refrigerating and Air-Conditioning Engineers Inc., 2001.
3. ESDU. Characteristics of atmospheric turbulence near the ground: Part 3-variations in space and time for strong winds (neutral atmosphere), Data Item 86010. London, Engineering Science Data Unit, 2001.

4. Fahrtash, M., Liu, H. (1990), "Internal Pressure of Low-Rise Building - Field Measurements", Journal of Wind Engineering and Industrial Aerodynamics, Vol. 36, pp. 1191-1200.
5. Ginger, J.D., Mehta, K.C., Yeatts, B.B. (1997), "Internal pressures in a low-rise full-scale building", Journal of Wind Engineering and Industrial Aerodynamics, Vol. 72, pp. 163-174.
6. Ginger, J.D., Holmes, J.D., Kim, P.Y. (2010), "Variation of internal pressure with varying sizes of dominant openings and volumes", Journal of Structural Engineering, ACSE, Vol. 136(10), pp. 1319-1326.
7. Ginger, J.D., Holmes, J.D., Kopp, G.A. (2008), "Effect of building volume and opening size on fluctuating internal pressure", Wind and Structures, Vol. 11, pp. 361-376.
8. Halkyard, R., Blanchard, G., Flay, R.G., Velychko, N. (2009), "Adaptation of tubing response correction filter coefficients to suit reduced sampling frequencies", Proceedings of the 7th Asia-Pacific Conference on Wind Engineering, Taipei, Taiwan.
9. Holmes, J.D., Best, R.J. (1981), "An approach to the determination of wind load effects on low-rise buildings", Journal of Wind Engineering and Industrial Aerodynamics, Vol. **7**, pp. 273-287.
10. Holmes, J.D. (1979), "Mean and fluctuating internal pressures induced by wind", Proceedings of the 5th International Conference on Wind Engineering, Fort Collins, Pergamon Press, Oxford, Vol. 1, pp. 435-450.
11. Holmes, J.D., Ginger, J.D. (2009), "Codification of internal pressures for building design", Proceedings of the 7th Asia-Pacific Conference on Wind Engineering, Taipei, Taiwan.
12. Holmes, J.D., Ginger, J.D. (2010), "Internal Pressures- The Dominant Opening Case- A Review", Proceedings of the 9th UK Conference on Wind Engineering, University of Bristol, UK.
13. Kwok, K.C.S., Hitchcock, P.A. (2009), "Characterisation of and wind induced-internal pressures in a compartmentalised building during a typhoon", Journal of Wind and Engineering, Vol. 6, pp. 30-41.
14. Liang, H., Li, L., Jian, F., Qinhan, F. (2006), "Coherency matrix-based proper orthogonal decomposition with application to wind field simulation", Earthquake engineering and engineering vibration, Vol. 5(2), pp. 267-272.
15. Lieblein, J., (1974), "Efficient methods of extreme value methodology", National Bureau of Standards Rep. No NBSIR 74-602, Washington D.C.
16. Liu, H., Saathoff, P.J. (1982), "Internal pressure and building safety", Journal of the Structural Division, Vol. 108, pp. 2223-2234.
17. Oh, H.J., Kopp, G.A., Inculet, D.R. (2007), "The UWO contribution to the NIST aerodynamic database for wind loads on low buildings: Part 3. Internal pressures", Journal of Wind Engineering and Industrial Aerodynamics, Vol. 95, pp. 755-779.
18. Rowan, Williams, Davies and Irwin, (1993), "Review of internal pressures on low-rise buildings", Report to Canadian Sheet Steel Institute, RWDI Report 93-270.
19. Sharma, R.N., Richards, P.J. (1997), "Computational modelling of the transient response of building internal pressure to a sudden opening", Journal of Wind Engineering and Industrial Aerodynamics, Vol. 72, pp. 149-161.
20. Sharma, R.N., Richards, P.J. (2003), "The influence of Helmholtz resonance on internal pressures in a low-rise building", Journal of Wind Engineering and Industrial Aerodynamics, Vol. 91, pp. 807-828.
21. Sharma, R.N., Richards, P.J. (2005), "Net pressures on the roof of a low-rise building with wall openings", Journal of Wind Engineering and Industrial Aerodynamics, Vol. 93, pp. 267-291.
22. Standards Australia/Standards New Zealand. Australian/New Zealand Standard Structural design actions, Part2: 2002 - AS/NZS 1170.2:2002. Standards Australia International Ltd., Sydney, AS and Standards New Zealand, Wellington, NZ, 2002.
23. Vickery, B.J., Bloxham, C. (1992), "Internal pressure dynamics with a dominant opening", Journal of Wind Engineering and Industrial Aerodynamics, Vol. 41, pp. 193-204.
24. Yu, Shi-ce, Lou, Wen-juan, Sun, Bing-nan (2008), "Wind-induced internal pressure response for structure with single windward opening and background leakage", Journal of Zhejiang University, Vol. 9(3), pp. 313-321.

NUMERICAL STUDIES ON EVALUATION OF AERODYNAMIC FORCE COEFFICIENTS OF CABLE-STAYED BRIDGE DECK

M. Keerthana[1], K.P. Jaya[2], S. Selvi Rajan[1], Hephzibah Thampi[3], and R. Ravi Sankar[3]

[1] Scientist, CSIR-SERC, Taramani, Chennai -113
[2]Assistant Professor, Anna University, College of Engineering, Guindy, Chennai-20
[3] Project Student, Anna University

ABSTRACT

The present study aims to evaluate the static aerodynamic force coefficients required for the design of cable-stayed bridge against wind loads. A section of a bridge deck model consisting of three T- beams as deck cross section, having a geometric scale of 1:50 was selected for this purpose. Simulation of the flow around bridge deck was done using Computational Fluid Dynamics (CFD), through ANSYS/FLOTRAN software package which discretises the governing equations based on finite element method (FEM). Different turbulence models along with suitable numerical techniques were used for this analysis. CFD calculations through discrete vortex method (DVM) were also carried out in the aero-class of software RM2006, which is used exclusively for design of bridges. The bridge deck model with anti-crash barriers was initially subjected to a uniform wind speed of 14 m/s. The static aerodynamic forces-lift, drag and moment - were computed for seven different angles of wind incidence acting across its longitudinal direction. The numerically obtained aerodynamic force coefficients from ANSYS/FLOTRAN and RM2006 were compared with the experimental results obtained based on boundary layer wind tunnel studies.

Keywords: Aerodynamic coefficients, Boundary Layer Wind Tunnel, Computational Fluid Dynamics, Discrete Vortex Method, Finite Element Method, Simulation, Turbulence

INTRODUCTION

The criteria for the design of long-span suspension bridges are concerned with static and dynamic response of bridges under wind loading. Traditionally, the analysis of a bridge under wind loading has been carried out using wind tunnel experiments on sectional models. Recently, with the advent of high power computing facilities, there have been major developments in the computational area due to which it is possible to numerically simulate flow fields and their effects on structures. In the present study, the 2-D model of a bridge deck cross-section is analysed to obtain the static aerodynamic forces of lift and drag, and moment using computational fluid dynamics (CFD). The plane airflow around an obstacle is generally described by the two-dimensional Navier-Stokes equations for incompressible fluids with constant viscosity. These governing differential equations in CFD are discretised using two of the most popular methods, namely, finite element method (FEM) and discrete vortex method (DVM). Discretisation of flow by FEM is available in ANSYS/FLOTRAN, while by DVM , it is available in RM2006 software. The aerodynamic forces are obtained from analysis in ANSYS/FLOTRAN, which primarily consists of arriving at the optimum mesh size, domain, and selection of suitable numerical algorithm and turbulence model. The in-built turbulence mode ls of ANSYS/FLOTRAN that were chosen for the analysis are Standard k-ε model, k-ω model and Shear Stress Transport model (SST). The discrete vortex method (DVM) which is available in the aero-class of RM2006, was used to arrive at the aerodynamic force coefficients. The results from the numerical studies are validated with the aid of boundary layer wind tunnel studies. The ability of DVM (which is relatively a

new technique) to predict the flow features around bridge deck section was also studied using the results from experiment.

AERODYNAMIC COEFFICIENTS

The forces per unit length F_x and F_y along the fixed body axes (x-axis and y-axis respectively) are computed using the measured pressures. The mean force coefficients in x, y directions are obtained as given below:

$$\overline{C}_{Fx} = \frac{\overline{F}_x}{B\left(\frac{1}{2}\rho\overline{U}_z^{\,2}\right)} \text{ and } \qquad \overline{C}_{Fy} = \frac{\overline{F}_y}{B\left(\frac{1}{2}\rho\overline{U}_z^{\,2}\right)}$$

where $\overline{C}_{Fx}$ $\overline{C}_{Fy}$ = mean force coefficient along x and y axes and B is the characteristic dimension which is taken as the height of the bridge section/the dimension normal to the flow for the present case. The resultant of the aerodynamic forces experienced by a structure subjected to wind action can be resolved into drag F_D, (along- wind) force acting in the direction of the mean wind and lift F_L, (across- wind) force acting perpendicular to the direction of the mean wind. By resolving F_x and F_y in the direction of wind and perpendicular to the direction of wind, the drag force F_D and the lift force F_L, respectively are obtained. Forces along drag and lift directions are computed based on the equations given below (Francesco 2002):

$$\overline{C}_D = \frac{\overline{F}_D}{0.5\rho\overline{U}_z^{\,2}B} \text{ and } \qquad \overline{C}_L = \frac{\overline{F}_L}{0.5\rho\overline{U}_z^{\,2}B}$$

The wind induced moments are the effects resulting from the normal forces on the bridge surface at top and bottom multiplied by their lever arms and integrated over the entire surface. Moment coefficient is computed from:

$$\overline{C}_M = \frac{\overline{M}}{0.5\rho\overline{U}_z^{\,2}B^2}$$

where

$\overline{C}_D$, $\overline{C}_L$, $\overline{C}_M$ = mean drag, lift force and moment coefficients, respectively

$\frac{1}{2}\rho\overline{U}_z^{\,2}$ = reference pressure at deck height, z, due to mean wind speed, $\overline{U}$ where ρ is the density of sir

NUMERICAL SIMULATIONS

The details of analysis carried out through FEM and DVM in order to obtain aerodynamic force coefficients are detailed below:

Finite Element Method (using ANSYS/FLOTRAN)

ANSYS/FLOTRAN is a computational fluid dynamics tool which works on the basis of finite element discretisation of the governing Navier-Stokes equation. The problem domain (a numerical wind tunnel test section) of length 1800 cm, width 250 cm and height 180 cm was considered for modeling. Cross-section of bridge deck, that is representative of existing full-scale cable stayed bridge in Goa, having width of 13.2 m, consisting of three T-sections was modeled to a scale of 1:50. The wind tunnel sectional model had a length of 98 cm, a width of 26.4 cm

and a deck thickness of 0.7 cm. Fig.1 shows the cross-section and dimensions of the bridge deck model, including direction of forces. The two dimensional representation of test section of the wind tunnel was meshed using unstructured mesh of quadrilateral elements (Fluid 141 model of ANSYS/FLOTRAN). Fluid 141 model is used in transient or steady state fluid systems that involve fluid or non-fluid regions. The conservation equations for viscous fluid flow and energy equation are solved in the fluid region, while only the energy equations are solved in the non-fluid region. Since the gradients are very high in the near-wall regions, the mesh that was obtained by free area meshing was further refined near the wall in order to obtain non-dimensionalized distance from the wall (y^+) in the range of 30 to 40. This ensures the adequacy of the mesh near the wall region and results in a dense mesh near wall and relatively sparse mesh away from the wall. Fluid properties like density ($1.226 kg/m^3$) and kinematic viscosity ($14.3x10^{-6} m^2/s$) were also simulated. For the discretised elements, the velocities are obtained from the conservation of momentum principle, and the pressure is obtained from conservation of mass principle. The following boundary conditions were given:

- Zero-slip and turbulence at the fluid-surface interfaces of the bridge deck
- Zero-slip at the top and bottom boundary of the problem domain
- Velocity at entry and pressure at exit

The bridge deck was assumed to be a rigid bluff body and subjected to uniform fluid flow with velocity of 14 m/s. The Reynolds number corresponding to the flow velocity is 55,000 (based on the dimension perpendicular to flow as characteristic dimension), which invokes the need for turbulence modeling. RANS (Reynolds Averaged Navier-Stokes) approach based turbulence models namely Standard k-ε model, k-ω model and Shear Stress Transport model (SST) are used, in which the effect of whole turbulence spectrum is modeled using eddy of a single characteristic length and time scale. A brief overview of these models is given below:

Turbulence Modeling

Standard k-ε model: The turbulent kinetic energy, k and the rate of dissipation of turbulent kinetic energy, ε are modeled and then these two values are used to define the velocity scale and the time scale, at any given point and time in the flow field as representative of large scale turbulence and to evaluate turbulent eddy viscosity. The rate of change of kinetic energy is related to the convection and diffusion of the mean motion of the flow (Keerthana and Harikrishna 2010). According to literature (Chung T.J. 2002, Ghoshdastidar 1998), Standard k-ε model usually provides a realistic picture of the flow in case of turbulent flow in pipes and channels. Though the formulation is robust, the standard k-ε model has shortcomings like over-prediction of turbulent energy k when applied to flow field with impingement, inability to resolve flows with large strains such as swirling flows and curved boundary layers flow.

Standard k-ω model: The standard k-ω model is very similar in structure to the k-ε model but the variable ε is replaced by the dissipation rate per unit turbulent kinetic energy (or) specific dissipation rate of turbulent kinetic energy,ω. The k-ω turbulence model has the advantage near the walls to accurately predict the turbulence length scale in the presence of an adverse pressure gradient. This allows better treatment in solving the flow near wall where the boundary layer is affected by viscous nature of the flow (Keerthana and Harikrishna 2010). But, k-ω model is much more sensitive to the free-stream turbulence levels than the standard k-ε model.

Shear stress transport model (SST model): SST model overcomes the problem of free-stream dependency of the k-ω model and over-prediction of length scales near the wall by k-ε model. Suitable blending functions are

multiplied with both the models so that, the value of blending function becomes zero at the boundary layer and has a value of one near the wall (Keerthana and Harikrishna 2010). It also accounts for the transport of the turbulent shear stress inside boundary layers by modifying the turbulent eddy-viscosity function. The purpose is to improve the accuracy of prediction of flows with strong adverse pressure gradient, as well as flow with pressure-induced boundary layer separation.

It was found that the models and algorithms are problem specific and no model can be stated as best for all problems irrespective of the boundary conditions. To achieve greater convergence, SIMPLEN algorithm (Modified Semi-Implicit Method for Pressure-linked equations) was chosen for pressure-velocity coupling based on literature survey (Larry 1984, Kazuori 1999, Panneer Selvam 2001). Wind incidence with seven different angles, namely, 0^0, $\pm5^0$, $\pm10^0$ and $\pm15^0$ to the horizontal direction of the bridge deck were considered. A turbulent analysis of the flow was performed until convergence. The pressure distribution, velocity streamline and pressure coefficients were found to predict as expected, i.e., the greater the angle of attack, the greater the lift. Integrated forces based on pressure distributions were arrived to calculate lift, drag and moment coefficients.

Discrete Vortex Method (using RM2006)

Discrete vortex method is a powerful and efficient computational technique for the simulation of two-dimensional viscous flows, particularly in cases involving flow separation and vortex roll-up. In a high Reynolds number flow, there are three regions namely the viscous, rational boundary layer and an inviscid outer region which is usually irrotational. In DVM, vorticity is introduced at a certain region or point and it is traced through the flow by means of vorticity equations derived from Navier-Stokes equation. The DVM technique uses Lagrangian framework to solve the Navier-Stokes Equations. The advantage of this approach is that it is a grid-free method and data input is much facilitated. Consequently, it does not impose further problems to consider also moving cross sections. The key-points of this method are:

- Representing the outline of the cross section by a number of straight lines/panels
- Representing the vorticity field by an ensemble of discrete vortex particles of given circulation and core size

RM2006 simulates wind tunnel numerically for evaluation of aerodynamic coefficients of lift, drag and moment using DVM.

Modeling Geometry: The Geometric Pre-processor (GP) of RM2006 allows to easily describe the structural model of the bridge deck cross-section, by defining axes in plan and elevation over which the geometry is modelled using extensive graphic input. The cross-section properties are assigned to the start and end of each beam element (along the span of the bridge) and the rest are automatically computed using a Finite Element (FE) approach. A consistent FE-mesh is a pre-requisite for the calculation of cross-section properties. Two-dimensional 9-noded iso-parametric elements (Lagrange elements) are used for the FE-calculation of the cross-section values (RM User Guide, 2007). The quadratic shape function used for these elements guarantees good behavior even with rather coarse meshes.

Modeling load: RM2006 provides simulated load type for wind in the form of distribution of mean wind velocity over the height, turbulence parameters and power spectrum parameters, to compute mean drag, mean lift and mean moment, in addition to which the user-defined parameters can also be given for wind load. Total wind loads had been separated into four components, each of them separately defined with the appropriate load type, namely forces

in longitudinal direction, forces in lateral direction, forces in vertical direction and moment around the element axis (Fig. 1). Additional parameters like, the density of air, the design velocity, time integration, number of iteration steps, size of vortex particles to represent turbulence, wind angle α, and the appropriate reference width were also defined. The viscosity of fluid is given as $15x10^{-6}$ m^2/s.

Analysis: To define the spatial resolution, the number of surface panels of 300 along the cross section contour and the size of the vortex particles of 0.087 are specified. The resolution is limited by the finite element mesh of the cross section. RM2006 performs CFD calculation for the modeled cross section and stores the resulting coefficients in the form of table containing aerodynamic coefficients of the respective aero class. They include force components in wind direction (drag, F_D) as well as normal to it (lift, F_L), and a moment around the element axis (moment, M). These aerodynamic coefficients are dependent on the wind angleα. As an additional function, RM2006 calculates time histories of the C_D, C_L, C_M coefficients and shows an animation of the airflow around the cross section. Discrete vortex method (DVM) is only used in this software for the calculation of aerodynamic data and also for studying/visualising the behaviour of bluff body wakes. The post processor provides the results of the mean values of drag, lift and moment for each wind angle from -15^0 to $+15^0$ including 0^0 wind angle.

WIND TUNNEL EXPERIMENT

Wind tunnel tests were carried out on the section model of a cable stayed bridge deck having the same cross section as used for CFD analysis, using Boundary Layer Wind Tunnel Facility at CSIR-SERC, Chennai (Structural Engineering Research Centre-Photo1). The pressure measurement test was conducted under simulated open terrain flow corresponding to a geometric scale of 1:50. All the pressure coefficients are deduced with respect to the reference dynamic pressure measured at the level of bridge deck. The force coefficients are evaluated based on pressure measurements. A computer program is written in MATLAB, for integration of pressures to evaluate aerodynamic coefficients, C_D, C_L, and C_M. The torsional moment, M, for all angles of attack with respect to origin of the cross section has been evaluated using the measured pressures along with their lever arms. The details of the test setup and procedure are explained elsewhere (Selvi, 2008).

RESULTS AND DISCUSSION

Figs. 2, 3 and 4 show the velocity streamlines around the bridge deck obtained from different turbulence models. Fig. 5 shows the flow pattern around the bridge deck obtained using DVM. For the results from boundary layer wind tunnel, a surface integral of the pressure was performed on the deck and the forces of lift, drag and moment were obtained. Variation of coefficients of drag, lift and moment with angle of wind incidence for the three chosen turbulence models of FLOTRAN/ANSYS, RM2006 and the wind tunnel results are shown in Figs. 6, 7 and 8, respectively. As the numerical analysis is carried out at a relatively smaller turbulence level, the mean values of aerodynamic coefficients based on experiment are only used for comparison.

The analysis on drag force showed that coefficient of drag was not a direct function of incident angle of attack (Ken-Chi-Maeda 1999). The values of drag coefficients arrived based on RM2006 matched well with the wind tunnel data exhibiting the better performance of DVM compared to finite element discretisation of governing equation with the use of all the other turbulence models used in the present study for CFD simulation. Among the three turbulence models used, Standard k-ε model is unable to capture the physical flow phenomenon, while Standard k-ω model and SST model performed better, which in turn is reflected by a reasonable prediction of mean

drag coefficients. It can be observed that the mean values of lift coefficients derived based on RM2006 compared well with the wind tunnel results, while those predicted by FLOTRAN/ANSYS show greater variations with reference to the experimental values, especially in case of negative angles of wind incidence. Figs. 7 and 8 clearly show that for negative angle of wind incidence, analysis using FLOTRAN/ANSYS estimated lesser values of lift coefficients and almost a constant value of moment coefficient for all wind angles. However, the slope of mean lift coefficient from the numerical analysis matches with the experiment. In case of moment coefficient, results from both FLOTRAN/ANSYS and RM2006 are under predicted compared to the experimental values. The difference in results may be attributed to the assumptions made in numerical analysis.

The values of lift and moment coefficient can either increase or decrease depending on dynamic vortices formed in the downstream end (Ken-Chi-Maeda 1999). The numerical technique must be able to capture the effect of the vortices in order to obtain results which represent the actual physics of the problem studied. In this direction, analysis using improved turbulence models and numerical schemes are required to obtain results that are close to wind tunnel experiments. The analysis also shows the ability of discrete vortex method to simulate well the flow around bluff bodies.

CONCLUSION

The forces exerted on a bridge structure by wind, assuming steady flow, depend on the size, the shape of the cross section of the bridge deck, the angle of attack and the velocity of the incoming flow. The flow-chart describing the steps involved in this present study is given in Fig. 9. All the analysis on the bridge deck model has been carried out by assuming the bridge deck as a perfectly rigid bluff body, without considering m induced effects. As can be seen from Figs. 6 to 8, the values of drag from both the analysis and measurement compare well. More reliable values can be observed in experimental results compared to numerical values for the cases of lift and moment coefficients, which is attributed to the gap in numerical techniques used. The variation of C_D and C_L from RM2006 matches very well with the values obtained based on wind tunnel tests, whereas moment coefficient does not match. The reliability of the numerical analysis for computation of C_M using RM2006 needs to be studied further. The numerical analysis using FLOTRAN/ANSYS assumes certain mathematical principles of geometry that is extremely complex and can give only approximate results compared to the exclusive software like RM2006 which is meant to be for analysis of bridges and demands more refinement in modeling of turbulence to increase the quality of numerical simulations. The paper shows the use of numerical analysis to obtain force coefficients for bridge deck sections, could be used to optimize the design and bring about the possibility of greater stability for the structure, without carrying out experiments during all the stages of optimization.

ACKNOWLEDGEMENT

This paper is being published with the kind permission of Director, CSIR-SERC, Chennai.

REFERENCES

1. ANSYS user's Guide. (2005). Documentation for ANSYS, Release 10.0.
2. Chung, T.J. (2002). "Computational Fluid Dynamics." Cambridge Univ. Press.
3. Francesco Ricciardelli. (2002). "Pressure Distribution, Aerodynamic Forces and Dynamic Response of Box Sections." J. of Wind Eng. & Ind. Aerodyn, Vol. 90(10), 1135-1150.
4. Ghoshdastidar, P. S. (1998). "Computer simulation of Flow and Heat transfer." Tata McGraw-Hill, New Delhi.
5. John D.Holmes. (2001). "Wind Loading of Structures." Spon Press, UK.

6. Kazuori Yamaguchi. (1999). “Field Observation and Vibration Test of Tartara Bridge.” Proceedings of IABSE Conference, Sweden, 707-714.
7. Ken-Ichi-Maeda. (1999). “Structural Countermeasures for Design of Very Long Span Cable-Stayed Bridge under Wind Loads.” Proceedings of IABSE Conference, Sweden, 224-233.
8. Keerthana, M., and Harikrishna, P. (2010). “Turbulence Models for Wind Engineering Applications-an Overview.” The seventh Structural Engineering Convention, SEC 2010, Annamalai University, 626-641.
9. Larry. J. Segerlind. (1984). “Applied Finite Element Analysis.” Wiley & Sons Inc.
10. Matlab user guide. (2004). Mathworks Release 14.
11. Paneerselvam, R., and Suresh Govindasamy. (2001). “A report on Aero elastic analysis of bridge girder section using computer modeling.” Mack Blackwell Transportation Center, Univ. of Arkansas.
12. Peter King, J. (2003). “The Aerodynamics of Long Span Bridges.” PhD Thesis, Department of Civil Engineering, UWO, Canada.
13. RM User Guide. (2007). TDV, Bentley.
14. Selvi Rajan, S. (2008). “Investigations into Aerodynamics of Bridges through Wind Tunnel Testing.” Ph.D. Thesis, CEG, Anna University.
15. Simiu and Scanlan. (1996). “Wind effects on structures: An Introduction to Wind Engineering, Third Edition.” John Wiley & Sons Inc.
16. Strommen, E. (2006). “Theory of Bridge Aerodynamics.” Springer, Netherlands.
17. Troitsky, M. S. (1977). “Cable Stayed Bridges: Theory and Design, Second Edition.” Crosby Lockwood Staples, London.

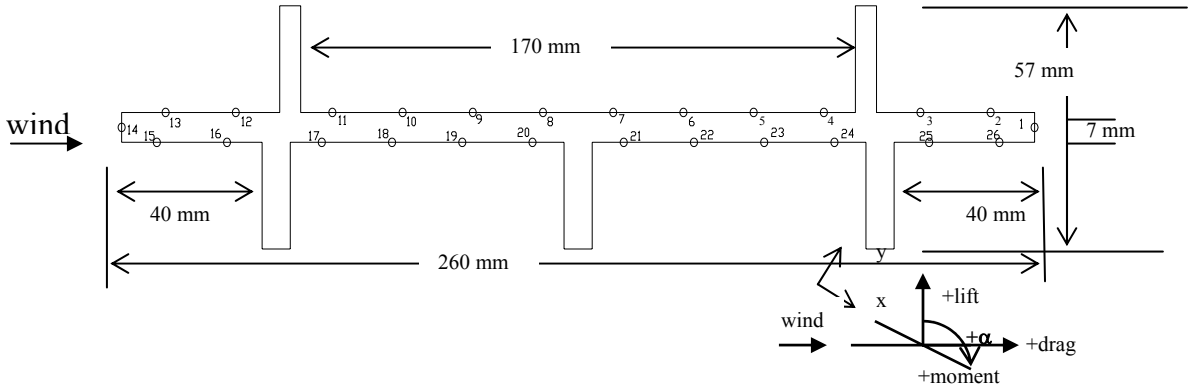

Fig. 1 Cross-section of the bridge deck model and the sign convention for force

Photo 1 Test set-up inside wind tunnel for 0^0 wind incidence

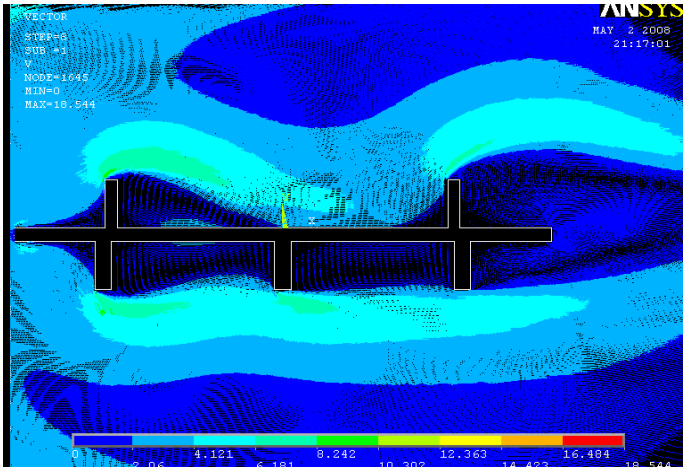

Fig. 2 Velocity streamlines around bridge deck using k-ω model

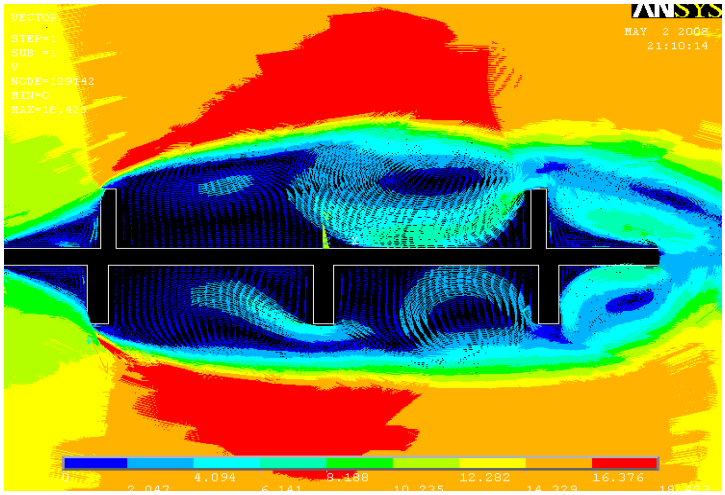

Fig. 3 Velocity streamlines around bridge deck using Standard k-ε model

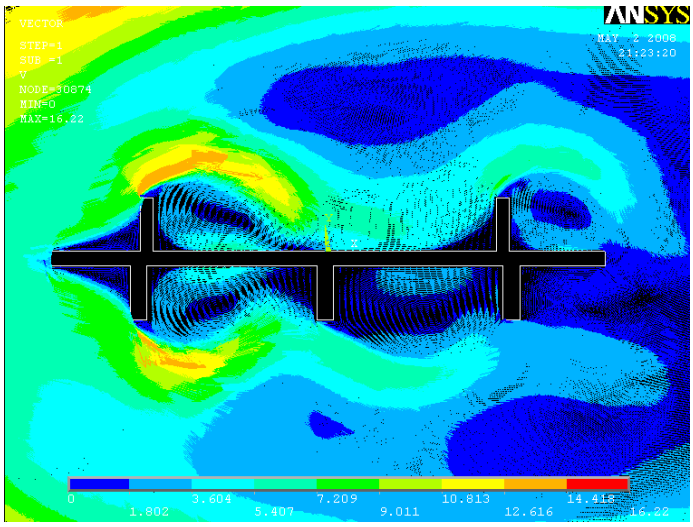

Fig. 4 Velocity streamlines around bridge deck using SST model

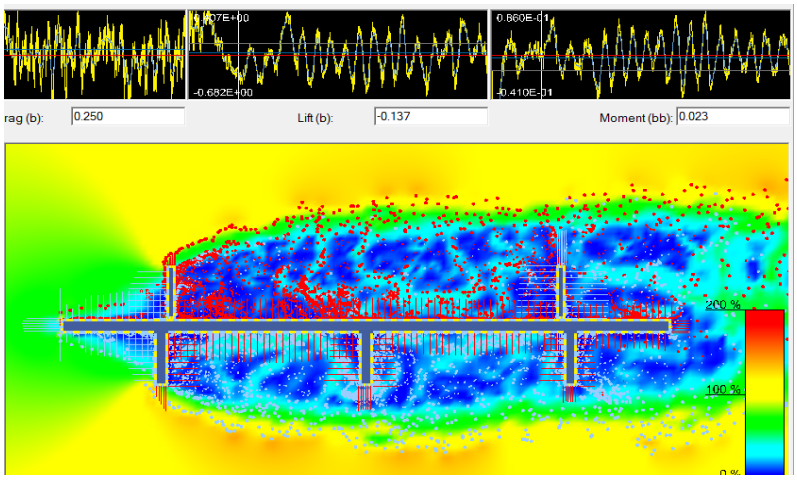

Fig. 5 Flow pattern around the bridge deck due to simulated wind load-RM2006

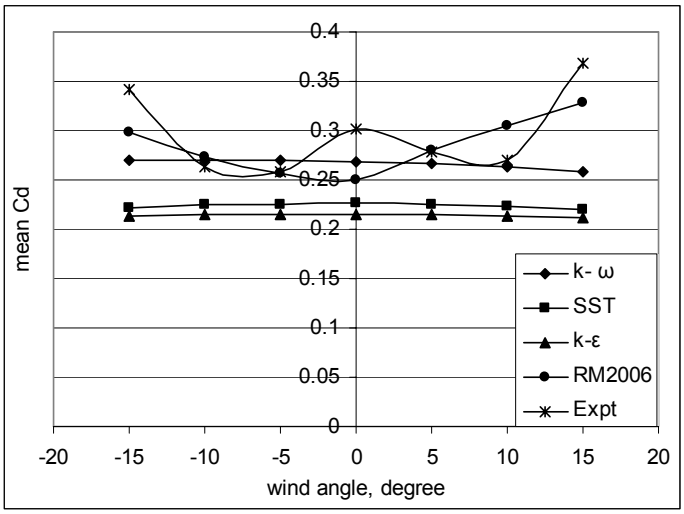

Fig. 6 Variation of mean drag coefficient with wind angle

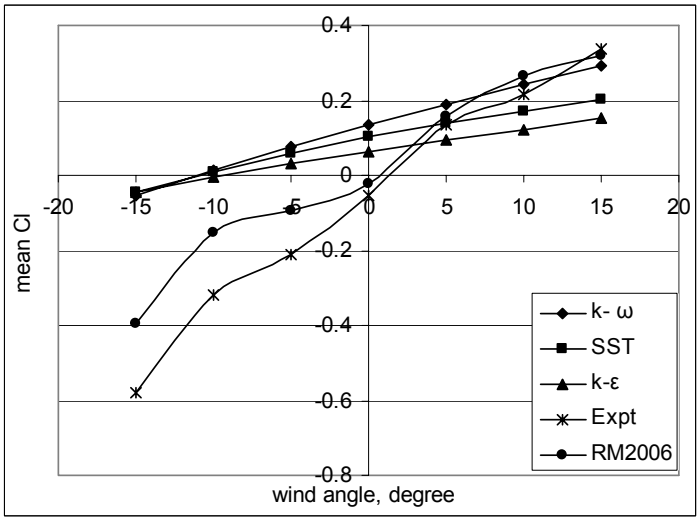

Fig. 7 Variation of mean lift coefficient with wind angle

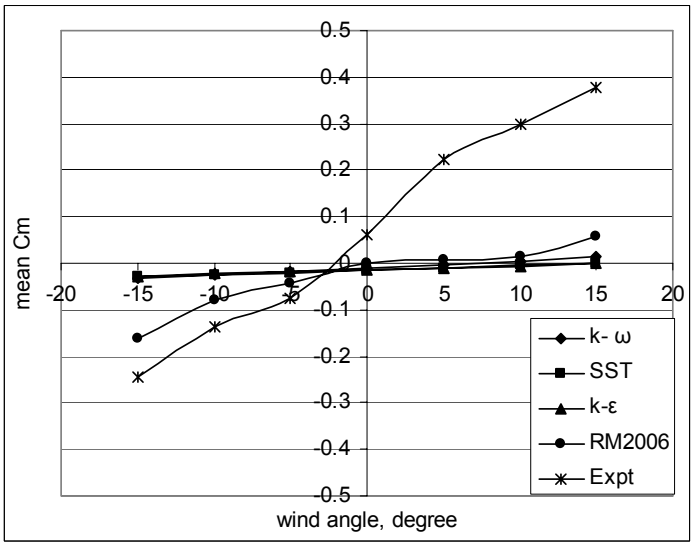

Fig. 8 Variation of mean moment coefficient with wind angle

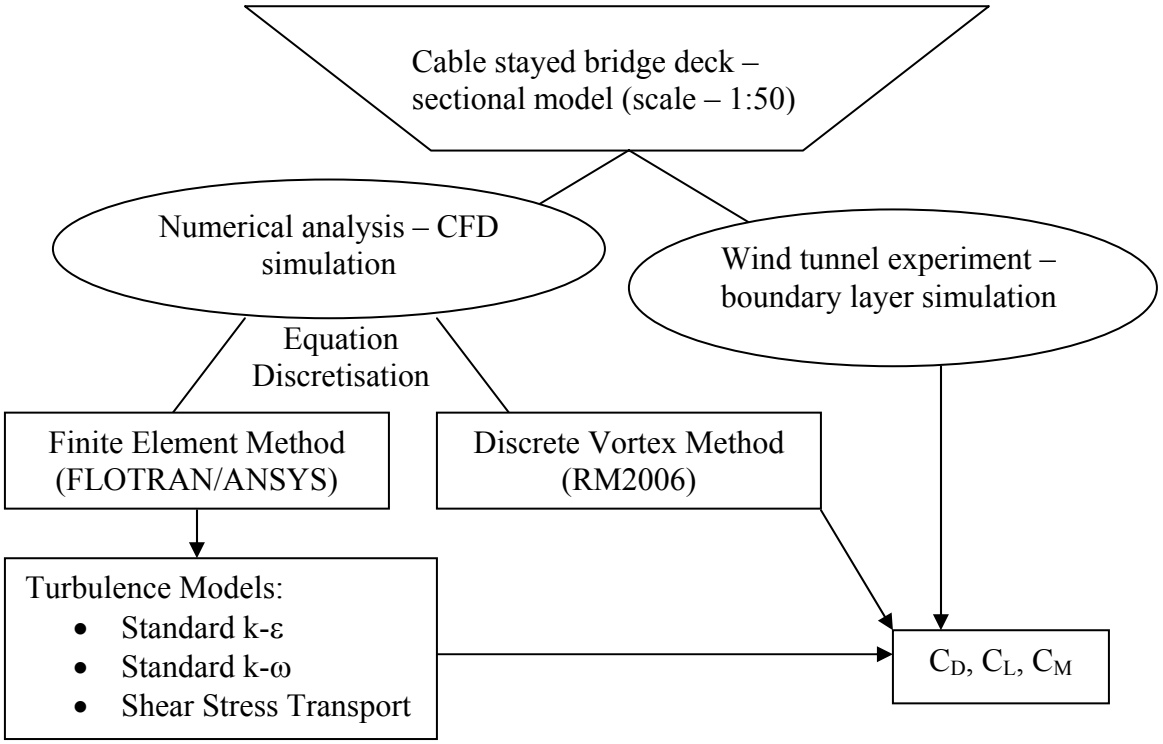

Fig. 9 Flow-chart describing the steps involved in the present study

CHARACTERISTICS OF SURFACE PRESSURES ON A BUILDING UNDER A TORNADO-LIKE FLOW AT DIFFERENT SWIRL RATIOS

Geetha Rajasekharan Sabareesh[a*], Masahiro Matsui[b], Yukio Tamura[c]

[a*, b, c] *Wind Engineering Research Centre, Tokyo Polytechnic University, 1583 Iiyama, Atsugi, Kanagawa 243-0297, Japan*
Tel& Fax: +81462429658;
[a*] - *Corresponding Author*

Email: [a*]sabareesh@arch.t-kougei.ac.jp, [b]masahiro@arch.t-kougei.ac.jp,
[c]yukio@arch.t-kougei.ac.jp

ABSTRACT.

Aerodynamic forces are induced on building surfaces when a tornado passes over it. To minimize the effect of tornadoes on structures, the characteristics of tornado-structure interaction should be clearly understood. Swirl ratio is a parameter that determines the nature and characteristics of a vortex flow. An attempt is made in the present investigation to determine the external surface pressures acting on a scaled building model engulfed in a stationary vortex when subjected to different swirl ratios. The tornado-like flow simulator at Wind Engineering Research Centre, Tokyo Polytechnic University was used to generate the stationary vortex. It is observed that the surface pressures on the building model are influenced by the effect of atmospheric pressure change at the centre of the simulator. At distances close to the radius of maximum winds, the building faces show differences in pressures.

Keywords: Swirl ratio, Forced vortex, tornado-simulator

INTRODUCTION

Many past studies [Mehta et al., (1976), McDonald et al., (1983)] have estimated wind loads on tornado-damaged buildings based on structural analysis. Lewellen & Lewellen (1997), Dutta et.al (2002), Selvam & Millet (2003, 2005) performed numerical analyses to compute tornado characteristics or resulting wind loads on structures. But in the past three-four decades there have been attempts to understand the mechanisms behind tornado-structure interaction by simulating vortex flows in the laboratory (Ward (1972)) and exposing building models to them to identify the behavior of buildings under a tornado-like flow regime (Jischke and Light (1983), Mishra et al. (2008), Haan et al. (2008), and Yang, Z et al (2011)). But the range of factors considered to be influencing the tornado-structure interaction was very limited.

Swirl ratio (S), which is the ratio of tangential to updraft flow rate in a tornado, is one such parameter that influences tornado-type flow both geometrically and dynamically (Davies- Jones (1973), Church et al (1979), P. Hashemi Tari et al (2010)). Depending on the swirl ratio, the nature and characteristic of the developed vortex can vary, which in turn influences the surface pressures on the building. In the present investigation, the surface pressures acting on a building exposed to a stationary tornado-like flow regime are investigated for a broad range of swirl ratios. A stationary tornado-like flow is one where there is no horizontal translation for the vortex. This situation can be compared to a very slow moving tornado in full-scale.

EXPERIMENTAL SETUP

A schematic of the stationary tornado-like flow simulator at the Wind Engineering Research Centre, Tokyo Polytechnic University, is shown in Figure 1. The vortex simulator consists of three main parts: a confluence region,

a convergence region and a convection region. Air is caused to flow in from the surroundings by generating a vertical updraft in the upper part of acrylic pipe (convection region) using a variable-speed fan. The updraft hole radius (*ru*) is 300mm. The core updraft flow remains nearly uniform across the updraft hole. A honeycomb structure is used as a flow-straightening device to remove vertically oriented vorticity. The confluence region is between the simulator floor and the updraft hole at the simulator periphery, through which flow enters the simulator. The surrounding flow is deflected to the simulator centre, the convergence region, through guide vanes at the simulator periphery, which can be adjusted to provide the required angular momentum to the incoming flow.

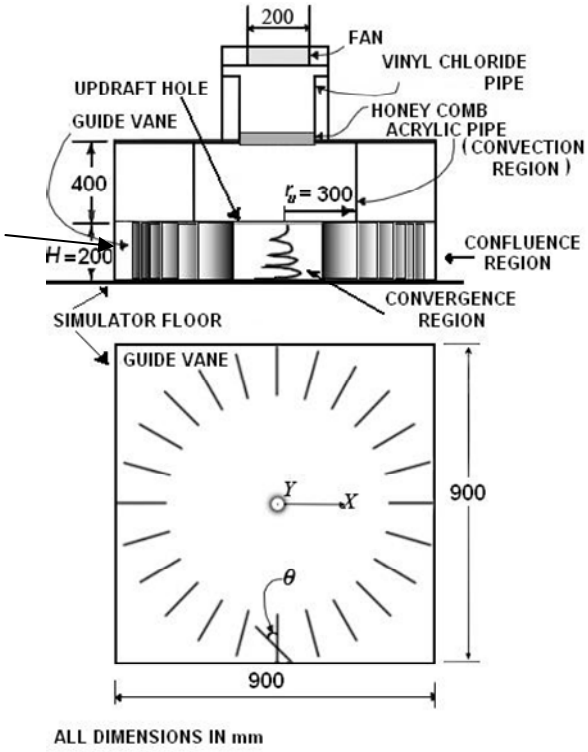

Figure 1. Schematic of tornado-like flow simulator

As shown in Figure 1, the orientation angles (θ) of the guide vanes were adjusted to obtain different swirl ratios. Swirl ratios are defined by the equation (Baker and Church (1979))

$$S = \tan\theta / 2.a \qquad (1)$$

where 'a' is the aspect ratio defined as the ratio of confluence region height to updraft hole radius. The range of swirl ratios used in the present investigation was 0.29~1.3.

The building model was a cube of side 25mm. The concept of the design tornado (Haan et al (2010)) based on comparison of the vortex core sizes of full scale to model scale tornadoes was used to establish the wind field scale. Previous investigations (Kobayashi. F et al (2007)) have observed the radius of tornadoes occurring in Japan to be of the order of 30m. The radius of the tornado obtained in the laboratory is of the order of 25~30mm. Thus, the wind field scale can be determined as 1:1000, so the cube model corresponds to a 25m cubic building in full scale, i.e., approximately of the size of a Gymnasium or a Nuclear power plant.

45 pressure taps were distributed evenly on the four side faces and roof face of the building model to capture the surface pressures. Data points were sampled at 700Hz. Obtained voltage signals were transformed to a time series of wind pressures. The effects of the tube system were removed.

Pressure values were then converted to pressure coefficients as follows.

The pressure coefficient (Cp_j) at any point (pressure tap)' j' is defined by:

$$Cp_j = (P_j - P_\infty) / q_r \quad (2)$$

Here 'P_j' represents the combined effect of static and dynamic pressures at the measuring point, 'P_∞' is the reference static pressure measured far from the vortex and 'q_r' is the reference dynamic pressure. Two definitions of dynamic pressures are used in the present study, and are explained in the corresponding sections.

RESULTS & DISCUSSIONS

FLOW VISUALIZATION

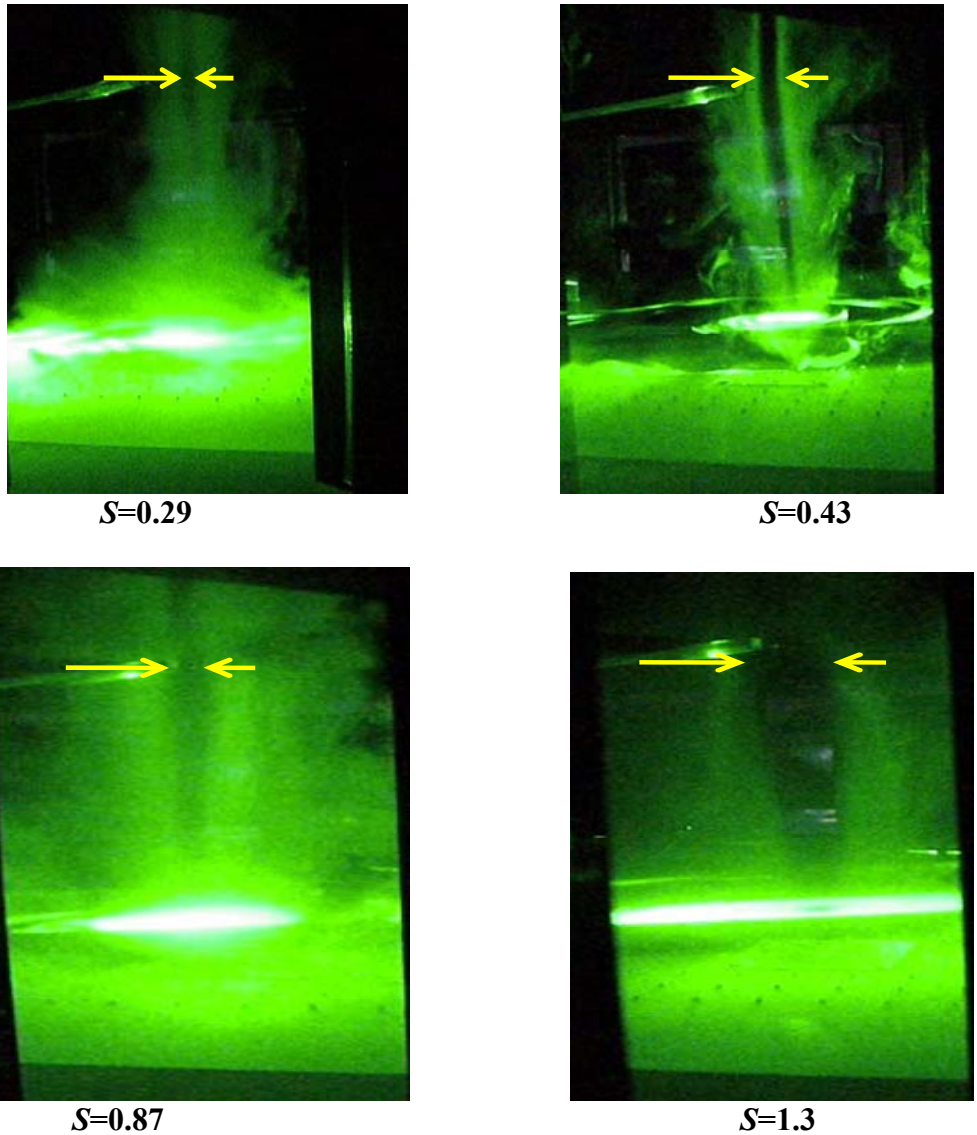

Figure 2. Flow Visualizations showing tornado central core for different swirl ratios

Water mist and a green laser arrangement were employed to visualize the flow on the simulator floor in the absence of the building model. By analyzing the effect of swirl ratio on the developed vortex core from the flow visualization shown in figure 2, it can be seen that the vortex core size increases with increase in swirl ratio.

This trend agrees well with some previous researches such as Baker and Church (1979).

Velocity Measurements

The response of the velocity field to the swirling flow determines the type of flow field in the simulator. The scalar components of velocity were measured at definite radial locations from the simulator centre to the periphery and simultaneously at five different heights above the simulator floor at these radial locations. A multi-channel thermistor type anemometer probe that can simultaneously measure the mean velocity components at different locations was used for this purpose.

The vortex core in the present investigation is defined as the region from the geometric centre of simulator to the point of maximum velocity. The velocity at each measurement point is normalized by the maximum velocity occurring in the flow-field. A well defined core region with gradual change in velocity as it nears the centre existed for a low swirl ratio (Figure 3(a)). As the angular momentum imparted to the flow increased with increase in swirl ratio, the boundary of the core region expanded with height.

At a very large swirl ratio S=1.3, the centre of the rotating column of air experienced very sharp velocity changes close to the simulator centre making it difficult to determine the exact boundary of the core region (Figure 3(b)). Farther from the core, the velocity showed a steady decrease for all swirl ratios.

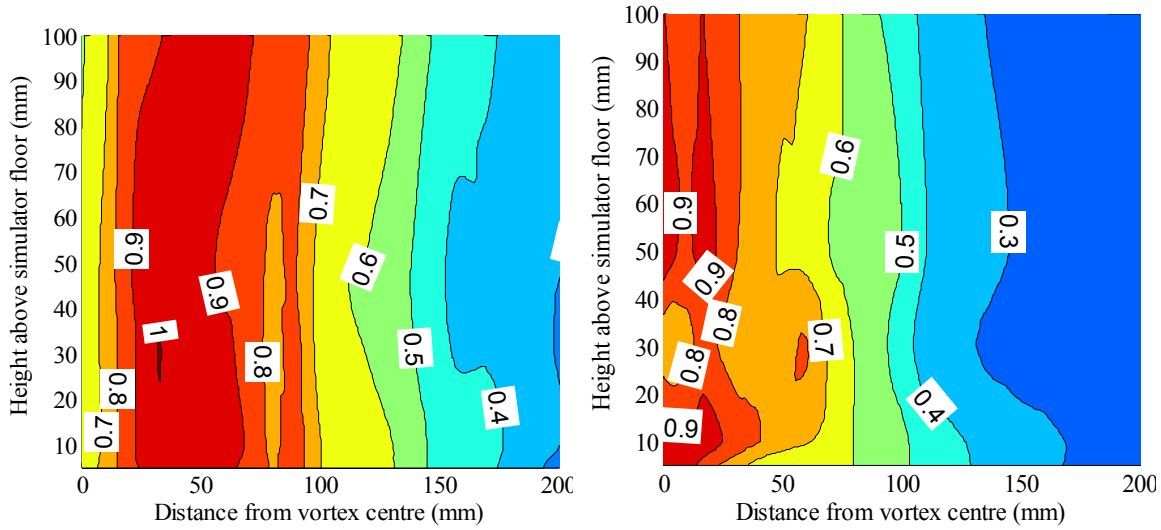

Figure 3. Velocity ($V/Vmax$) distributions with height on simulator floor for different swirl ratios (a) S =0.29 (b) S=1.3

PRESSURE MEASUREMENTS

Simulator floor

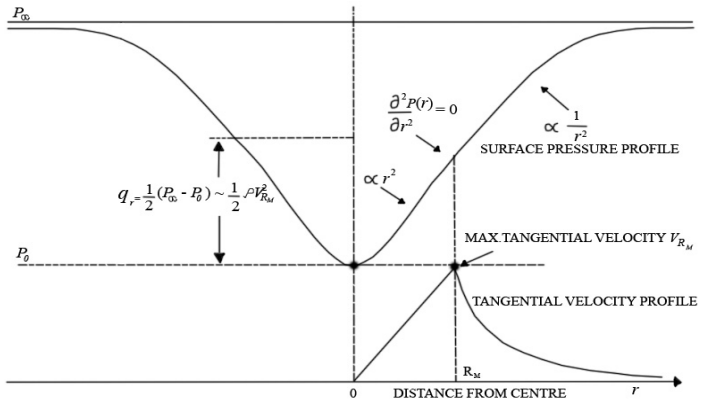

Figure 4. Definition of reference pressure

To compare the central pressures for two swirl ratio cases, reference dynamic pressure was chosen as half the centre pressure depth for the higher swirl ratio case. Assuming Rankine-Vortex behavior, this value is equal to $\frac{1}{2}\rho V R_M$ at the radius of the maximum tangential velocity (R_M), as shown in Figure 4.

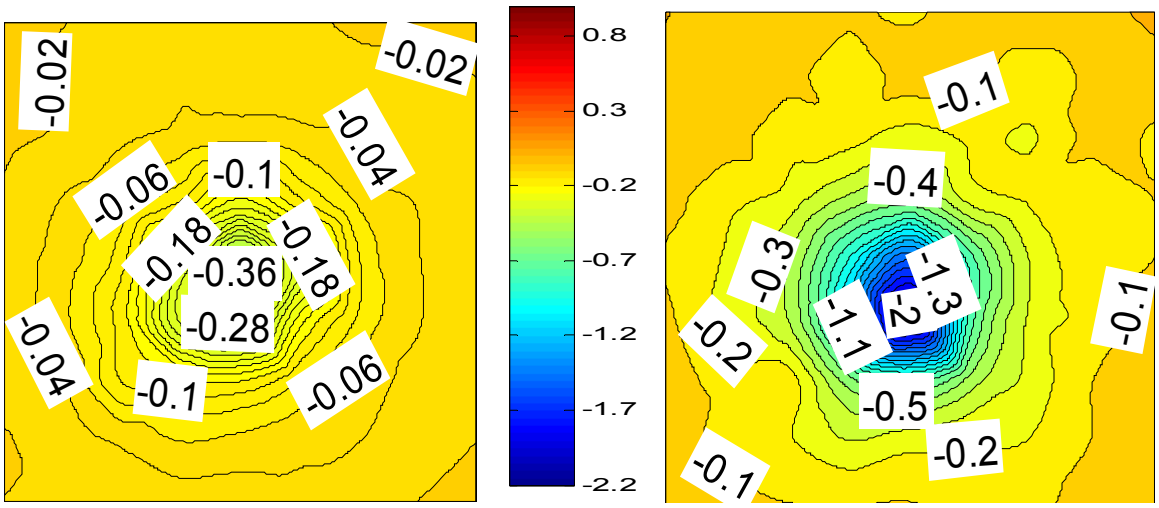

(a) (b)

Figure 5. Pressure distribution on simulator floor (a) *S* =0.29 (b) *S*=1.3

The pressure taps were distributed uniformly on the simulator floor from the centre to 1/3rd of the distance from the periphery to capture the pressure acting on the simulator floor under a tornado-like flow. There were a total of 81 pressure taps located at definite intervals on the floor, which were connected to a scanivalve pressure sensor, thus simultaneously measuring pressures at these points.

The distribution of mean pressure coefficients on the simulator floor was in the form of concentric circles, with the centre experiencing greater negative pressures, as shown in Figure 5. The negativity at the central core region increased with increase in swirl ratio.

Static and dynamic pressure change with introduction of building mode 1

Tornado-like flow is a very complex phenomenon where the ambient static pressure changes at every point. The situation becomes more complex with the presence of a building, which alters the flow suddenly. Thus, the effect

due to static and dynamic pressures needs to be separated and studied. To analyze this, the pressure values on the simulator floor (ambient pressure) without the building model were subtracted from those with the building model, which yields the residual component as shown in Figure 6. It can be seen that with the cube model, the flow pattern changes with respect to the ambient pressure, as evident from the difference in residual component. Here the pressure coefficients are defined as in Figure 4. At the periphery, this difference is very small, whereas in the building vicinity, it suddenly drops, and at the roof centre, the residual pressure shows less negative values.

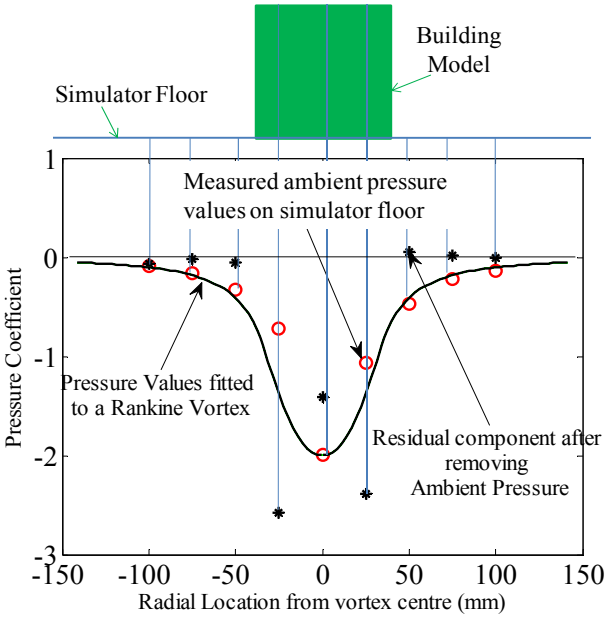

Figure 6. Effects of atmospheric pressure change at *S*=1.3

Mean pressure coefficients at critical points on building surface

The effect of swirl ratio on some critical points on the building model surface were analyzed and compared with the core pressure deficit. The definition of pressure coefficients was the same as in Figure 4. The dynamic pressure for the higher swirl ratio case (S=1.3) was used as the reference dynamic pressure (q_r) for all cases and the reference static pressure remains the same for all cases and is defined as in equation (2). Thus, in this section, the measured pressures (P_j) defined by equation (2) at the selected points on the building surface at different swirl ratios are compared. The cube was located at the vortex centre. The leading and trailing edges respectively were the leading and trailing edges of the cube to the clockwise tornado-like flow.

As can be seen from Figure 7 for the four different swirl ratios analyzed, the central pressure deficit on the floor without the building model showed a decrease with increase in swirl ratio. The pressures on the cube surface generally showed a tendency to decrease with increase in swirl ratio. The roof centre experienced higher negative minimum pressure at all swirl ratios. The difference in roof central pressure with the central pressure deficit on the floor increased with increase in swirl ratio. The roof centre experienced suction pressures 1.25~1.75 times the core pressure deficit. Also, the cube trailing edge pressures were (2~3 times) less negative than the roof pressures. The leading edge of the building model to the clockwise flow experienced suction pressures with magnitudes between the roof centre and central pressure deficit on the floor, and at higher swirl ratios these approached the magnitude of the roof central pressures.

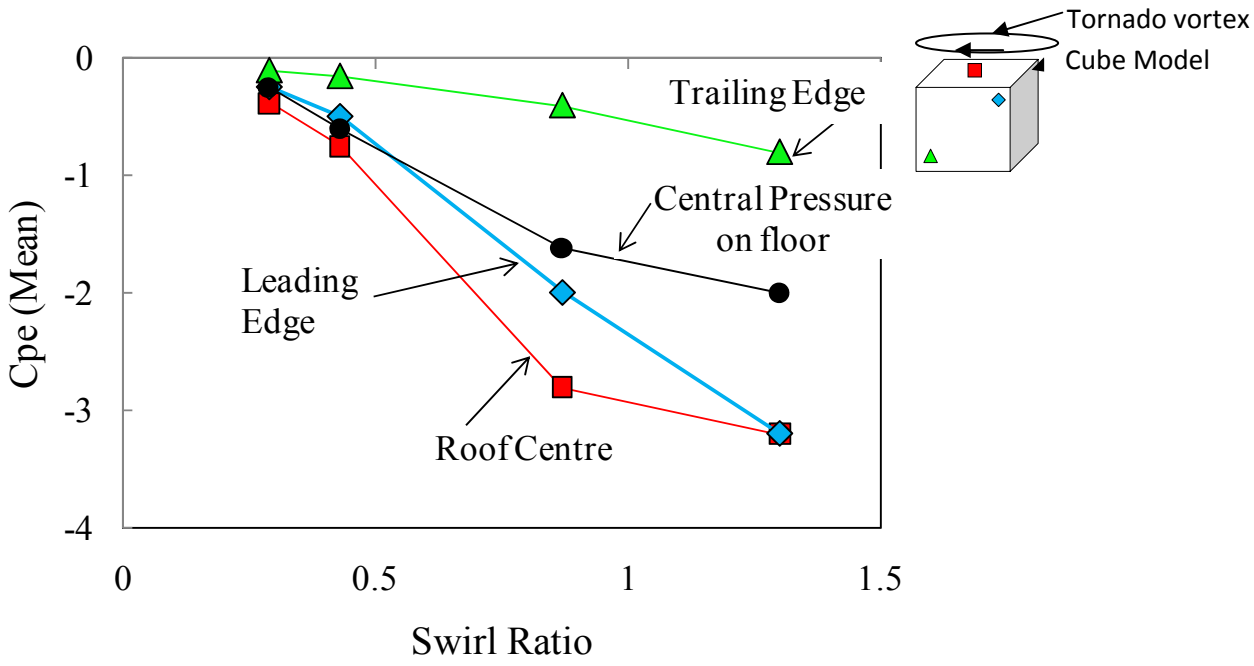

Figure 7. Comparison of mean pressures at different points on a cube with central pressures on floor

Behavior of building inside vortex core boundary

The mean pressure coefficients on the cube faces in the present investigation agreed with results of some previous studies (Mishra et al (2008b)) when the pressure coefficients were defined similarly as was done by these authors, who nevertheless reported pressure coefficients on building surfaces for a single swirl ratio case.

To understand the behavior of the building inside the vortex core boundary, the pressure coefficients on different building faces need to be analyzed. In the present investigation, to compare the swirl ratio effects on different building faces, the reference dynamic pressure (velocity pressure) was defined as $\frac{1}{2}\rho V^2$, where 'V' is the velocity measured at the corresponding building roof height, unlike the definition of dynamic pressure in the previous sections. The roof experienced *Cpe* (*mean*) of the order of -6 ~ -8.5 for the range of swirl ratios examined. These values were higher than those on the building walls at lower swirl ratios and became comparable at higher swirl ratios (see Figure 8). At higher swirl ratios the leading edge of the cube to the clockwise flow experienced comparable pressure coefficients to the roof corners. This is because the updraft flow remained almost constant for the entire swirl ratio range, whereas the tangential velocity increased with increase in swirl ratio. Thus, at lower swirl ratios, the vertical velocity predominates over the tangential velocity, whereas at higher swirl ratio, they become comparable. At all swirl ratios; the trailing edge experienced similar *Cpe* (*mean*) of about -2.

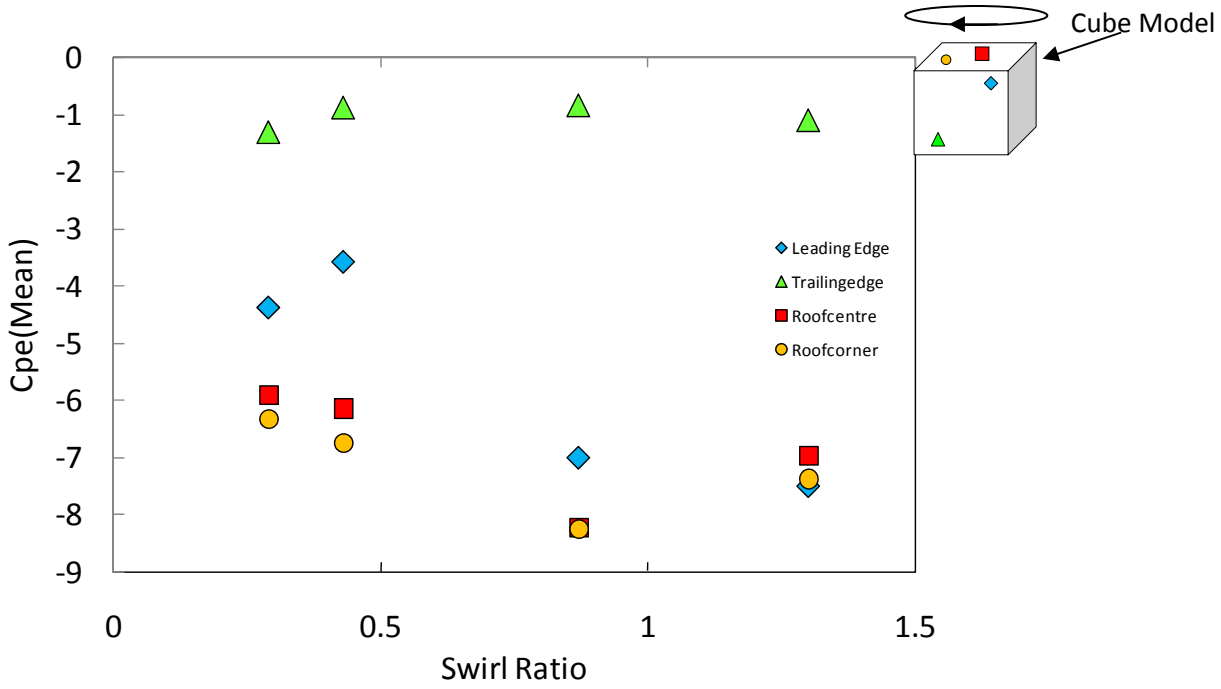

Figure 8. Mean pressure distribution at different swirl ratios

By analyzing the exploded faces of the cube model, Figure 9, it is observed that there exists axi-symmetry in pressure distributions on opposite sides. The axi-symmetric nature of the pressure distribution exists because the leading edges of the building model to the clockwise flow behave as separation regions, as is evident from the very negative pressures existing along the leading edges compared to those along the trailing edge of the cube. At lower swirl ratios, the difference between leading and trailing edge pressures were less, and progressively increased with increase in swirl ratio. With increase in swirl ratio, the tangential flow gained strength, as can be seen from the rapid variation of pressures spatially along the cube face and also the closer distribution of constant pressures lines on different faces of the cube.

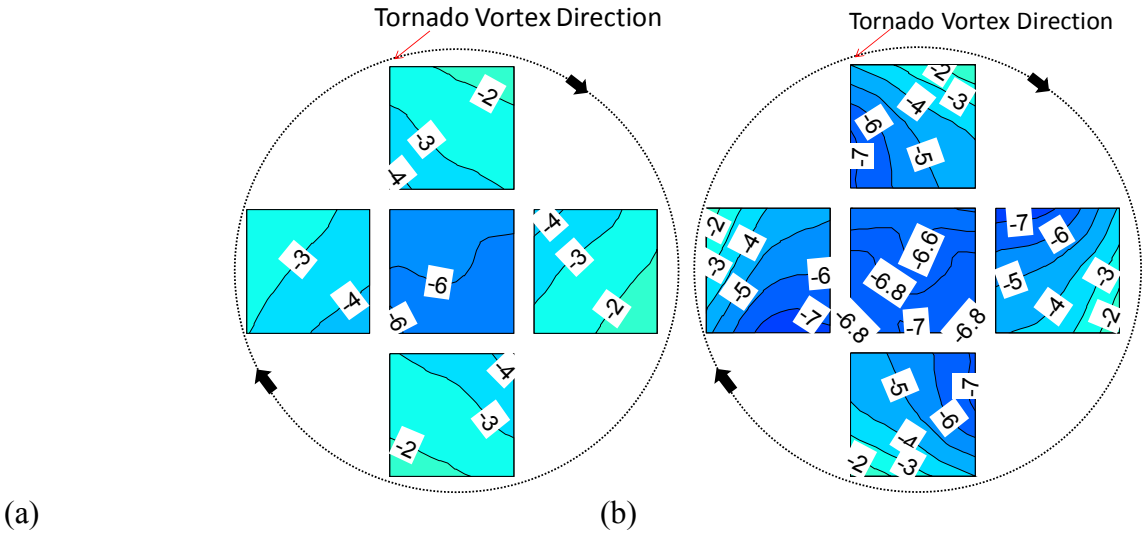

Figure 9. Mean pressure distribution on exploded face of cube (a) *S* =0.29 (b) *S*=1.3

At locations close to the core boundary, which correspond to regions of maximum winds, the effect of tangential flow on building faces A and C (see Figure 10) perpendicular to it started diminishing, resulting in lower suction pressures than those on the faces in line with the tangential flow (faces B and D). Comparing the minimum peak pressure coefficients (worst pressure

coefficients) on each face, see Figure 11, when the cube model is stationed near the vortex core boundary, the faces in line with tangential flow, B and D, experienced greater suction pressures comparable with the roof pressures, as these regions continue to remain as separation regions in the clockwise flow whereas faces A and C act as windward and leeward faces, respectively, for the flow perpendicular to these faces. Thus, face 'A' experiences lower suction than face 'C' at this location.

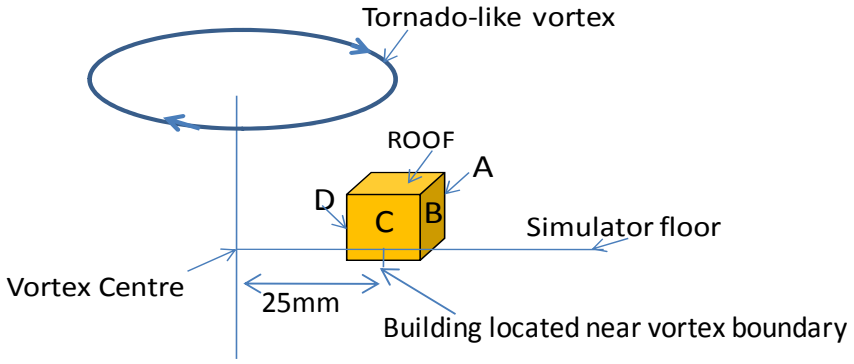

Figure 10. Building model with different faces shown

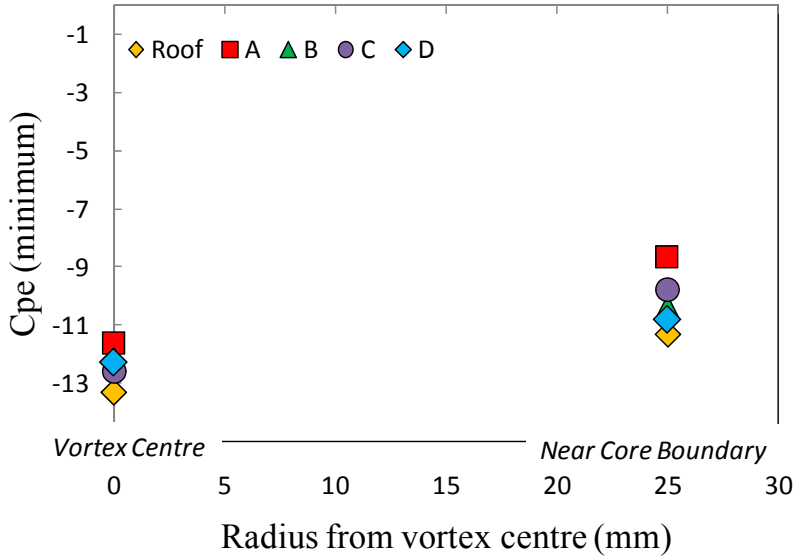

Figure 11. Minimum peak pressures on different faces for two locations of building model

CONCLUSIONS

(1) Central pressures on ground were distributed concentrically and the higher swirl ratio case caused lower central pressures.

(2) The presence of building model on ground significantly changed the pressures over and across the model, whereas there was much less change far from the building.

(3) Compared to the ground central pressures, the leading edges of the cube to the clockwise flow showed higher negative pressure coefficients and trailing edges showed less negative pressure coefficients at all swirl ratios. The roof centre also experienced greater negative pressure coefficients of the order of 1.25~1.75 times the central pressure deficit.

(4) Tangential velocity remained weak compared to the core updraft, resulting in lower suction pressures on building walls compared to those on roofs for lower swirl ratios, which progressively approached and became comparable with roof pressures with increase in swirl ratio.

(5) When the building was moved near the core boundary, which corresponds to the radius of maximum winds, the faces perpendicular to tangential flow experienced lower suction compared to faces in line with the flow.

REFERENCES

1. Baker, G.L., Church, C.R., 1979. Measurements of core radii and peak velocities in modeled atmospheric vortices. Journal of Atmospheric Sciences, 2413-2424.
2. Church, C.R., Snow, J.T., Agee, E.M., 1979. Characteristics of tornado-like vortices as a function of swirl ratio. A Laboratory Investigation, American Meteorological Society, 36, 1755-1774.
3. Davies Jones, R.P., 1973. The dependence of core radius on swirl ratio in a tornado simulator. Journal of Atmospheric Sciences, 1427-1430
4. Dutta, P.K., Ghosh, A.K., Agarwal, B.L., 2002. Dynamic response of structures subjected to tornado loads by FEM. Journal of Wind Engineering and Industrial Aerodynamics, 90, 55-69.
5. Haan, F.L., Jr., Balaramudu, V.K., Sarkar, P.P., 2010. Tornado-induced wind loads on a low rise building, Journal of Structural Engineering, 106-116.
6. Hashemi Tari, Pooyan; Gurka, Roi; Hangen, Horia, 2010, Experimental investigation of tornado-like vortex dynamics with Swirl ratio: The mean and turbulent flow fields, Journal of Wind Engineering and Industrial Aerodynamics, 98, 936-944.
7. Jischke, M.C., Light, B.D., 1983. Laboratory simulation of tornadic wind loads on a rectangular model structure. Journal of Wind Engineering and Industrial Aerodynamics, 13, 371-382.
8. Kobayashi, F, Sugimoto, Y, Suzuki, T, Maesaka, T, Moteki, Q.2007. Doppler radar observation of a tornado generated over the Japan seacoast during a cold air outbreak, Journal of the Meteorological Society of Japan, Vol 85(3), 321-334.
9. Lewellen, W.S., Lewellen, D.C., 1997. Large eddy simulations of a tornado's interaction with the surface. Journal of Atmospheric Sciences, 54(5), 581-605.
10. McDonald, J.R., Marshall, T.P., 1983. Report of damage survey of the tornadoes near Altus, Oklahoma on May11, 1982. Wind Science and Engineering Research Center, Texas Tech University.
11. Mehta, K.C., Minor, J.E., McDonald, J.R., 1976. Wind speed analysis of April 3-4 tornadoes. Journal of Structural Division, ASCE, 102(ST9), 1709-1724.
12. Mishra, A.R., James, D.L., Letchford, C.W., 2008a. Physical simulation of a single-celled tornado-like vortex, Part A: Flow field characterization. Journal of Wind Engineering and Industrial Aerodynamics, 96, 1258-1273.
13. Mishra, A.R., James, D.L., Letchford, C.W., 2008b. Physical simulation of a single-celled tornado-like vortex, Part B: Wind loading on a cubic model. Journal of Wind Engineering and Industrial Aerodynamics, 96, 1258-1273.
14. Selvam, P., Millet, P., 2003. Computer modeling of tornado forces on buildings. Wind and Structures, 6 (3), 209–220.
15. Ward, N.B., 1972. Exploration of certain features of tornado dynamics using a laboratory model. Journal of Atmospheric Sciences, 29, 1194-1204.
16. Yang, Z., Sarkar, P.P., Hu, H., 2011. An experimental study of a high-rise building model in tornado-like winds. Journal of Fluids and Structures, 27(4), 471-486